POLITECNICO DI TORINO

SCUOLA DI DOTTORATO

Dottorato in Meccanica – XXVI ciclo

Tesi di Dottorato

Development of a Clutch Assisted Engine Start

Enabling Stop & Start Sailing on next generation powertrain

Gianmarco Brunetti

Tutore
Prof. Giovanni Belingardi

Coordinatore del corso di dottorato
Prof. Luigi Garibaldi

Marzo 2014

A papá

Indice

Aknowledgements

The research has been conducted within General Motors Powertrain - Europe. I would like to thank Ing. Maurizio Cisternino, my company tutor, for supervising the work and for strongly believing in the outcomes of the project.

My deep appreciation and regard to Prof. Giovanni Belingardi for supervising my Ph.D program and acting as mentor both for my life and career.

Abstract

Environmental protection and efficient energy utilization have been always important issues in the automotive industry, but have gained significant momentum with the growing demand for mobility around the world and its impact on the global environment. For this purpose, many improvements in automobile technology have been accomplished over the past decades. However fuel economy with improvements in vehicle powertrain technology has been penalized by customer preferences. Automotive industry faces the challenge of producing vehicles that meet future fuel economy and emissions requirements which are priced to meet the desired customer value.

As hybrid vehicles, due to the high cost of the electrification they introduce, in next years will not impact the OEM fleet-averaged CO_2 figures in a significant way, it is beneficial to introduce new cost-oriented CO_2 features able to optimize engine operations, as they offer a very favorable cost/benefit ratio.

According to market trend, the increasing interest on automated transmission (i.e. AMT, DCT) plays a key-role towards the optimization of engine operation. The basic principle of shutting the engine off at idle to remove engineâs drag torque could be adopted at vehicle in motion, extending the distance covered by the vehicle coasting, when no traction is required, by opening the clutch automatically. Literature calls such operation âsailingâ: represents a low cost control feature, as it does not introduce new components, able to enhance Start & Stop technology.

Turning off the combustion engine during coasting conditions increases the number of engine starts over vehicle lifetime, impacting the whole vehicle.

Today starter motors are typically designed for Start&Stop applications for up to 300.000 engine crank over vehicle lifetime. This number can double for Start&Stop Sailing applications. However, the number of load cycles for the starter motor can be reduced significantly if the engine is revved up via clutch.

The work focuses on the development clutch assisted start by applying a new methodology based on modeling and simulation.

In general, starting the engine through clutch engagement consists in spending a certain amount of the traveling vehicle kinetic energy to spin up the engine. The consequent deceleration of the vehicle, due to this maneuver, must be mitigated by an

appropriate clutch closing strategy. Moreover, vibrations induced in the powertrain during the maneuver can generate uncomfortable feelings for the passenger.

Hence a powertrain and driveline modeling that allows to investigate the impact on drivability for different clutch engagement in different operating conditions in order to fulfill drivability requirements.

Capitolo 1

Optimizing HEV powertrain design to achieve CO_2 targets (5)

In recent years the pursuit of extremely low CO_2 emissions has gathered interest by OEM due to a combination of legislative and market requirements. In particular the European Commission mandate for 95 gCO_2/km in 2020, as well as a set of market incentives, which favor fuel efficient vehicles, is creating a strong request for technical solutions that may be applied in the OEMs portfolio in order to rapidly impact the fleet overall emission.

Hybrid Electric Vehicles (HEVs) can be considered one of the most promising ways of improving the sustainability of the road transport sector. They are equipped with an Internal Combustion Engine (ICE) coupled to an electro-mechanical system. Legislation offers an opportunity in developing parallel-hybrid powertrain featuring a direct electric drive and, optionally, an *off-vehicle charging*disposal. This layout allows to perform pure electric range, achieving a benefit in the computation of fuel economy (ECE Regulation No. 101).

Although Hybrid Electric Vehicles (HEVs) can be considered a viable technology to transition from conventional mobility to electric-mobility, their diffusion is still limited due to high costs. Technologies, in general, in order to become mass-production products should meet cost requirements, including the integration on vehicle. Automotive industry faces the challenge of producing vehicles that meet future fuel economy and emissions requirements which are priced to meet the desired customer value. Therefore, this chapter will present a methodology to optimize the design of a HEV powertrain, of its electric components and the vehicle mass in order to achieve CO_2 emission targets by using a meta modeling approach. Starting from a base diesel powered architecture, parameters focus of the optimization include base vehicle curb mass, battery size, degree of hybridization. For all architectures, selected by a DoE approach, calculated results includes additional cost to base architecture, CO_2 (according to EU norms), distance performed in pure

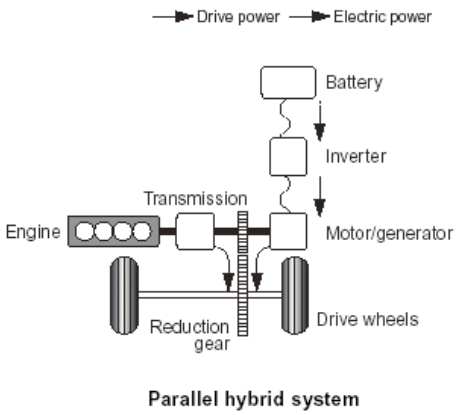

Figura 1.1: Layout of the considered hybrid powertrain

electric, hybrid functionalities (i.e. pure electric mode, regenerative braking, AWD mode). Parameters optimization is performed by empirical target function, based on gathered results.

After model definition, optimization investigates the most efficient way to achieve given fuel economy targets, expected functionalities, minimizing the additional cost of the architecture. An efficient way to achieve fuel economy targets for a mid-size class vehicle is proposed as the best compromise between all the analyzed targets. Final investigation evaluate the impact of adoption of lighter materials for BIW on the achievement of CO_2 targets.

1.1 Model definition

Increasingly stringent requirements for lower CO_2 emissions and the demand for a diversification of energy carriers are driving the development of future vehicles. In mid to longer term, evolutionary propulsion technologies with significant numbers in global vehicle fleet will impact on global fuel consumption and emission reductions. Emerging technologies such as electrification, in combination with optimized ICE have proved that the reductions in fuel consumption and emissions could be attained. However, the higher cost of the technology than traditional powertrain is limiting the impact on the fleet-averaged CO_2 figures in a significant way.

Among conventional powertrain, diesel engine are naturally more fuel efficient than gasoline, as reported in (3). Despite this advantage, it is becoming difficult to meet the increasingly stringent emission standards in a cost-efficient way. Therefore,

the analysis will focus on diesel powertrain as the higher diffusion in the European market in the mid-size and mid-size compact segments impacts the fleet-avereged CO_2 figures significantly and as their lower fuel economy and their higher production cost makes diesel a worst case for hybridization, reducing space for improvement by electrification (i.e. lower FE improvement, higher cost of the powertrain).

The study adopts a metamodeling design approach, allowing the comparison of different powertrain technologies, electrification architectures and BIW materials. There are a few significant differences between conventional and hybrid electric vehicles in terms of their powertrain components. Firstly, hybrid powertrains require additional components, such as electric motors, power electronic devices, and high-voltage battery packs. Secondly, they typically need modified design for the existing components (e.g. a smaller engine) because they have a new set of components. Lastly, some of the hybrid powertrains adopt novel configurations that utilize their components in a considerably different way from conventional ways. All these changes have to be carefully managed for the vehicles to be able to achieve performance that is close to their potential.

The purposes of employing metamodels in this study are manifold. It enables the adoption of numerical optimization techniques without using scaling of a baseline design. One favoured way in architectural studies is picking the best design *off-the-shelf*. This can refer to selecting among either different technologies or different size levels. Optimization techniques are essential in order to explore the vast design space with respect to engine and battery size as well as powertrain configurations and use light-weight materials for BIW. The optimization formulations includes cost for components and set penalty on emissions.

The metamodels developed are based on a mathematical, statistical approach with the aim of providing performance information of in-between designs, thus making it possible to use continuous design variables in the optimizations. In order to select candidates for a model set-up, the study adopts a DoE approach: candidates selection has been performed via optimal designs, allowing parameters to be estimated without bias and with minimum-variance; the criterion adopted is $V-$optimality, based on prediction variance, which seeks to minimizes the average prediction variance over a set of n specific points.

1.1.1 Design Variables

The first step towards optimization of the design of an HEV architecture is to define the main targets of the design.

HEV type The state-of-art technology of HEVs has brought to the market diverse hybrid architectures: literature has defined a main criterion to list architecture in 3 main categories according to the source of energy providing motion to the vehicle:

- series HEV â only EM drives the vehicle
- parallel HEV â both EM and ICE drive the vehicle
- seriesparallel HEV â allowing both previous layout

Both literature and market data have proven that a parallel HEV architecture represent the most promising technology for light-duty passenger cars. A suitable parameterization to investigate architecture accounts for the type of parallel HEV focusing on position of the EM in the powertrain. Tabella1.2 reports the value of the HEV type index according to the layout, described in Figura1.2.

Figura 1.2: Hybrid powertrain layout according to the type of parallel HEV.

Index	HEV type	HEV layout
1	Parallel	EM linked to ICE
2	Parallel	EM linked to gearbox
3	SeriesParallel	EM combined in transmission
4	Parallel	EM linked to separate driving axle

Tabella 1.1: The HEV powertrain layout

DoH	Electric Power	Electric Storage	Grid Recharge	Pure EV	Drive Range Limit
Mild HEV	Low	Very low	No	0%	Fuel
Full HEV	Med	Low	No	10%	Fuel
Plug-in HEV	Med	Med	Yes	30%	Fuel + Battery
EREV	High	High	Yes	70%	Fuel + Battery

Tabella 1.2: Attributes of Electrical Vehicles (1)

Degree of Hybridization Literature calls the increase in electrical content and magnitude onto the vehicle âelectrificationâ, indicating the development and integration of systems and components that enable electric energy to be used for transportation.

Hybrids have been traditionally classified by the amount of driving power supplied by the electrical system and the amount supplied by the engine. HEVs with large electrical systems and very small engines, this definition works pretty well. It also works relatively well for vehicles that do not have a downsized engine and have simply added on a technology referred to as an integrated starter generator: these are just conventional vehicles that can turn the engine off when the vehicle is stopped.

Both the amount of electrification and features supplied by electrification define the degree of hybridization on board of the vehicle.

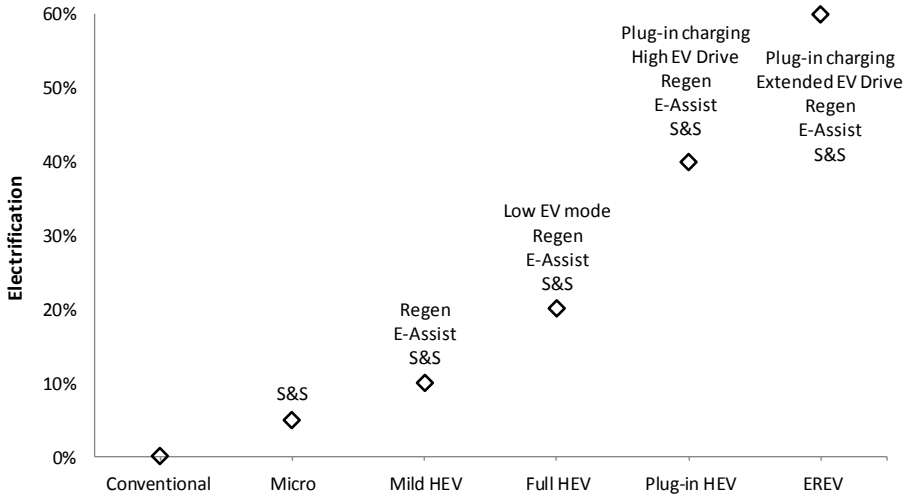

Figura 1.3: The amount of electrification at each degree of hybridization.

Battery size Lithium-ion batteries have become the standard for electric vehicles that store energy from the grid because of their superior energy density compared to other technologies. Batteries are mainly controlled by their SOC: in order to preserve their state of health through operations, they are usually limited in charging/discharging, therefore limiting the energy storage capabilities. Considered size of batteries and range of use of SOC are reported in Tabella1.3.

Degree of Hybridization	Energy kWh	SOC range %
S&S	0	0
Mild	0.5	0.3
Full HEV	2	0.5
Plugin HEV	4	0.5
EREV	16	0.5

Tabella 1.3: Energy content, usable SOC range of batteries according to the degree of hybridization of the powertrain

Vehicle size The goal of the methodology is to optimize cost of hybridization for a specific vehicle, therefore the model includes the size of the vehicle as a design parameter/control parameter.

The analysis refers to vehicle in major segments for European market Tabella1.4 in their baseline diesel powered configuration. Mass for type approval certification, so called Inertia Weight Class is reported as well.

Segment	Size	IWC kg	Base powertrain
B	1	1250	Small Diesel
C	2	1360	Mid-Sized Diesel
D	3	1470	Large Diesel

Tabella 1.4: Vehicle segmentation

Displacement Hybridizing a diesel powertrain provides significant fuel economy improvements over a conventional gasoline vehicle. However, these fuel economy benefits are subject to emissions, cost and degree of hybridization. Therefore, optimizing the design of a diesel-hybrid vehicle represents a greater challenge and assumes higher significance when looking at the European market.

Electrification offers opportunities for engine downsizing according to the degree of hybridization. The engine displacement describes the size of an engine. Moreover, according OEMsâ trend to reduce manufacturing costs by adoption of equal cylinder set (i.e. bore and stroke) for any ICE, downsizing is performed by reduction of the number of cylinders.

All powertrain considered must fulfil EU 6 emission levels, by adopting after-treatment disposals. Tabella1.5 reports engines evaluated in the study.

Size	Cylinders	Power kW	Displacement cm^3]
X-Small	2	45	800
Small	3	70	1200
Mid	4	95	1600
Large	4	115	2000

Tabella 1.5: Main data of ICE focus of the analysis

ICE contents Due to the high cost of electrification, OEMs lately tend to optimize baseline engine by introducing new contents to reduce diesel emissions and engine frictions, to enhance performance and warm-up.

A proper design of the powertrain towards CO_2 emissions reduction considers the introduction of ICE contents, in order to quickly compare electrification to conventional ICE improvement. Only for the purpose of the study 2 different contents have been analyzed: one reducing engine friction, one enhancing performarce. The model can consider any specific ICE content for evaluation.

Mass Reduction A major point of the analysis is to evaluate the impact of a mass reduction of BIW, by introduction of new materials and technologies for BIW (12).

Though enhancing energetic efficiency of powertrain, electrification implies a mass increase of the vehicle due to electric components (i.e. motors, batteries), leading to an higher energy request of the vehicle to complete a certain mission profile. As showed in 1.1, mass (m) impacts the the power required (P_{req}) by the vehicle during accelerations phases (P_{acc}). Resistive power (P_{res}) is calculated by use of coast-down coefficients.

$$\begin{aligned} P_{req} &= P_{res} + P_{acc} \\ P_{res} &= (F_0 + F_1 \cdot v + F_2 \cdot v^2) \cdot v \\ P_{acc} &= m \cdot \frac{\Delta v}{\Delta t} \cdot v \end{aligned} \tag{1.1}$$

In the design of electric components, i.e. battery, a proper trade-off between vehicle mass increase and battery size is defined in order to achieve CO_2 target, distance in pure EV mode.

The introduction of a light-weight design both mitigates the increase of vehicle mass due to electrification and leads to lower CO_2 values that might significantly impact fleet-averaged CO_2 figures.

Design Output

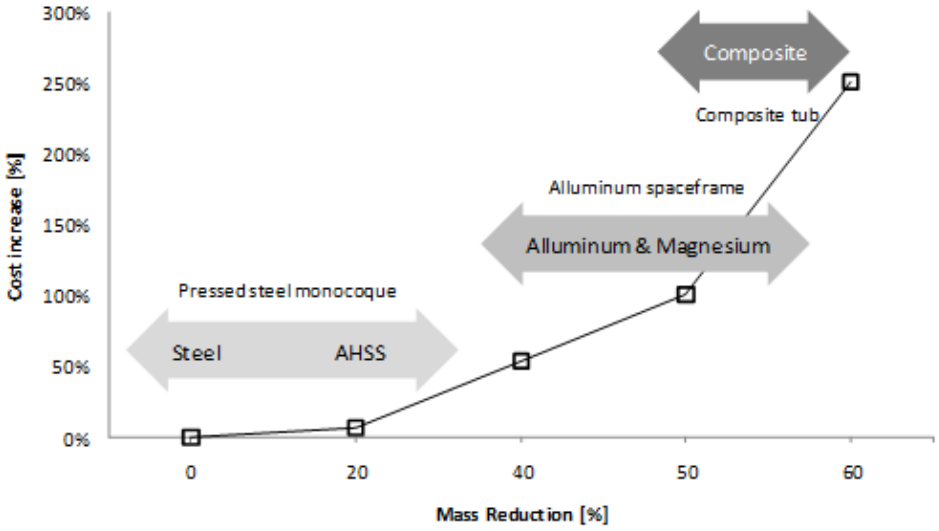

Figura 1.4: Impact on costs of technologies for mass reduction of BIW.

CO_2 emissions The main target for hybridization is the reduction of CO_2 emissions both to deliver better fuel economy .to customers and to achieve regulated emission compliancy.

Fuel economy for any selected architecture has been evaluated via simulation[1][2].

[1]Models for HEV powertrain include an optimization logic, so called Hybrid Operating Strategy (HOS): it provides for determining an overall value of mechanical power to be delivered to the wheels of the motor vehicle, for splitting this overall value in a first contributing value of mechanical power to be requested to the ICE and a second contributing value of mechanical power to be requested to the electric motors. In greater details, the splitting of the above mentioned overall power value is determined by minimizing the power losses due to the operation of the hybrid powertrain. Power losses are accounted in a predetermined polynomial function, usually referred as target function, which quantifies a quantity of power supplied to the hybrid powertrain through the ICE fuel, but not delivered to the wheels(3).

[2]CO_2 figures for Hybrid vehicles are calculated according to ECE Regulation No. 101, therefore measured on type approval homologation cycle. For PHEV, EREV only CO_2 value is evaluated by averaging the emissions of a cycles performed with fully-charged battery with the ones performed at minimum SOC. Then each emission value is weighted as follows: $M = \frac{D_e \cdot M_1 + D_{av} \cdot M_2}{D_e + D_{av}}$, where D_e is the distance performed in pure EV mode and D_{av} is an average value between 2 charges set by regulations to 25km.

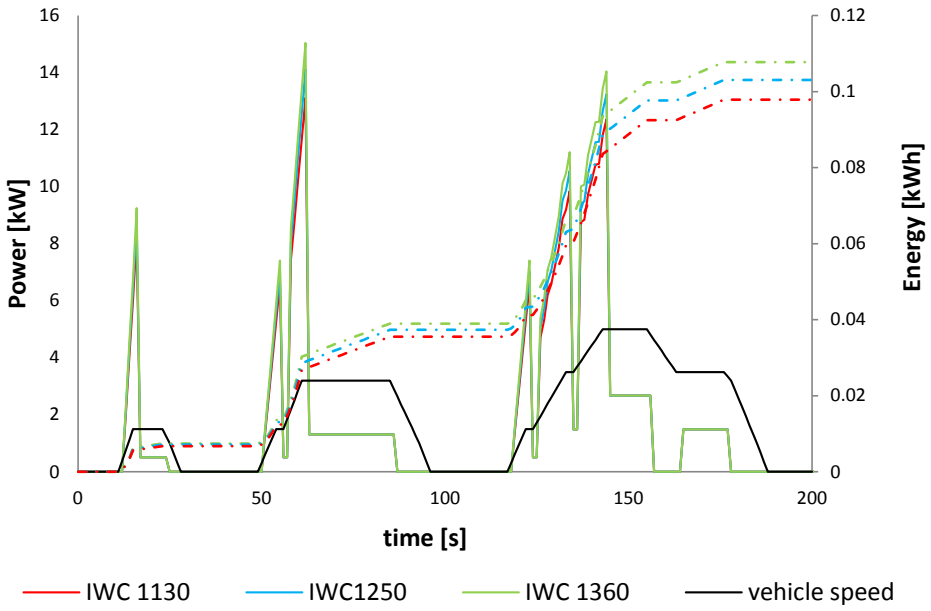

Figura 1.5: Impact of vehicle mass on energy, power required over NEDC homologation cycle.

Modelling and simulation of Fuel Economy, emissions The model is based on a âquasi-staticâ approach: even though the fuel consumption and emissions are calculated as functions of the dynamic ICE speed and load profiles, each condition is based on experimentally-derived stationary maps.

The model was assessed by means of experimental tests carried out at the dynamic test bed and at the roller test-bench by means of prototype vehicles, at GMPT-E test facilities.

Mass The vehicle mass represents a main driver towards the reduction of CO_2 emission. Electrification increases the mass of the vehicle, lowering, therefore, the fuel economy improvements. Though, the introduction of new technologies and materials for BIW offers a good opportunity to contain mass increase due to electrification and battery size for electrification

Performance Performance are represented by an index of adequacy for the powertrain design for a given platform. Starting from an architecture 0, represented by the proper base engine match for vehicle size Tabella1.6, an engine upgrade/downgrade increases the index by ± 1 (Figura1.6).

Vehicle Size	Displacement [cm^3	Power kW	Performance
B	1200	70	0
C	1600	95	0
D	2000	115	0

Tabella 1.6: Architecture 0 for balanced performance.

Performance index is affected by mass reduction, battery size, engine contents, type of hybridization.

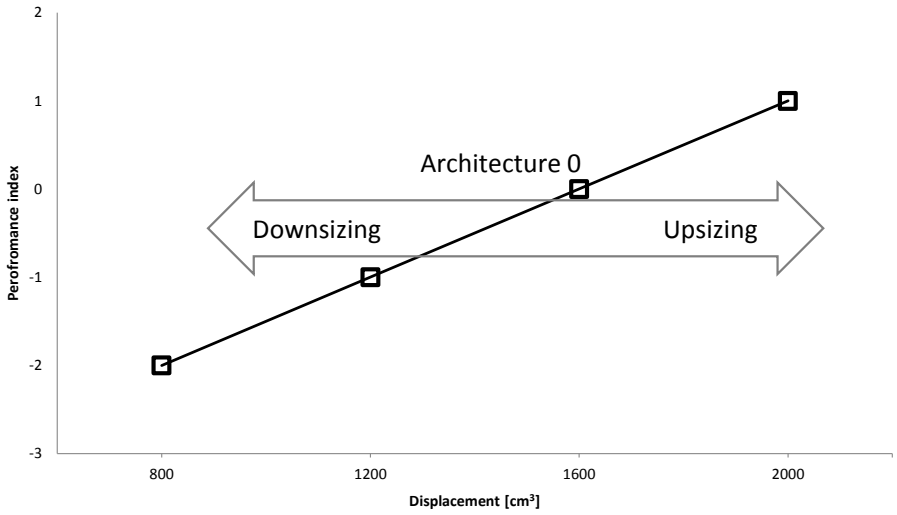

Figura 1.6: Index of performance: impact of engine displacement.

Functionalities Any vehicle should fulfil to certain requirements or expectation from the customer. Electrification, according to the selected architecture, offers the opportunity to develop new functionalities for the vehicles. The study considers:

1. Stop & Start - engine shut-off when no traction is requested
2. Electric boost â electric assistance to ICE
3. Pure EV mode

4. All wheel drive

Index Vale	Functionalities
1	S&S
2	S&S, Electric boost
3	S&S, Electric boost, Pure EV
4	S&S, Electric boost, Pure EV, AWD

Tabella 1.7: The functionality index.

Cost It accounts for the cost of the whole electrification and materials for BIW, compared to the same vehicle in the baseline configuration. As goal of the study is to achieve emissions compliancy in the most cost efficient way for OEMs, this parameter is the one minimized according to given constraints. All design parameters impact cost in different ways (Figura1.7).

Electric Range Besides contributing in the computation of CO_2 emissions for HEVs, the increasing focus on electric mobility, more stringent regulations to access city-centre in major cities, make electric range an important target for HEVs. The distance to be covered in a pure EV mode represents one of main criteria in the design of vehicles for future mobility. The study evaluates through simulations the electric range according to type approval procedures described in ECE Regulation No. 101 (4).

Electric range mainly depends on the size of batteries, i.e. the amount of energy stored, for a given hybrid architecture.

1.1.2 Design of Experiment

A full factorial combination of all design parameter leads to a large amount of combinations to evaluate via simulation. The DoE seems the right approach as it reduce the number of simulations run, considering both combination of effects and eliminating unfeasible combinations of design parameters for instance full electrified vehicles with small batteries.

Matlab-based âModel based calibrationâ tool has been adopted to design experiments, limiting the space of variation of parameters, by introduction of specific constraints. For instance, Figura1.8 shows that vehicles might introduce further engine downsizing only at high degree of hybridization.

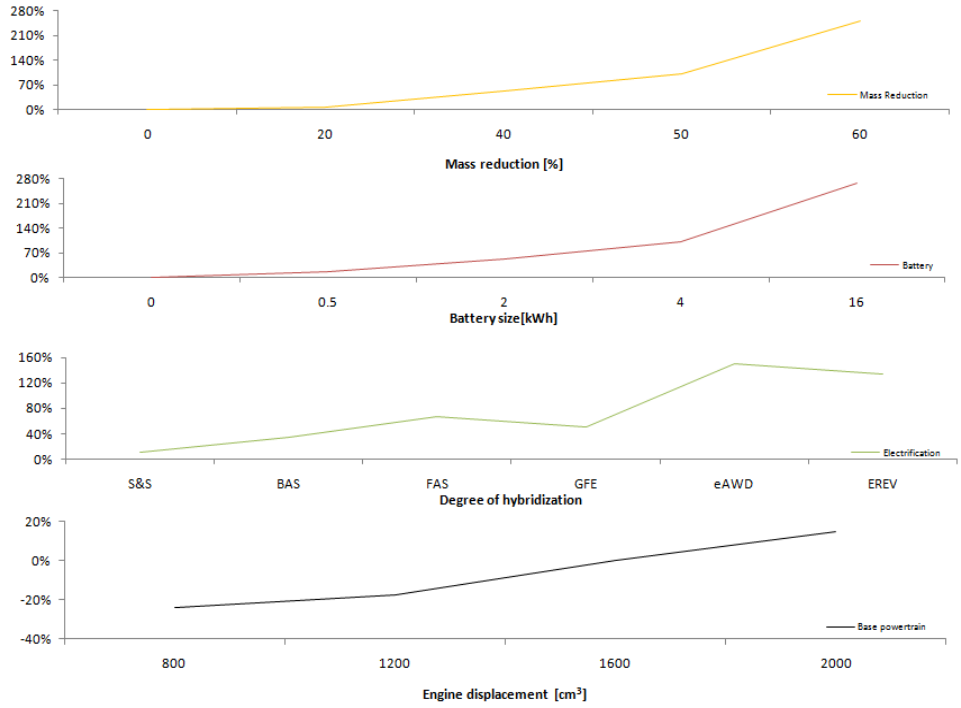

Figura 1.7: Cost increase according to vehicle design parameters.

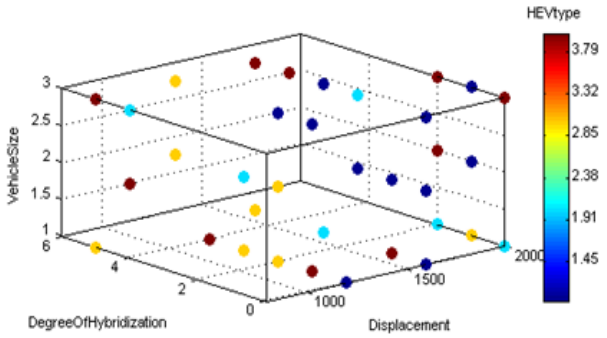

Figura 1.8: 4D projection of experiments for the design.

The model built from test results uses second grade polynomial functions 1.2. It results that design output are linearly correlated to input design parameters.

$$(CO_2, Cost, Functionality, Performance, Mass, EVrange) = \\ f\left(HEV^2_{type}, DOH^2, \%\quad mass\quad reduction^2, Size^2_{ICE}, Size^2_{veh}, ICEcontent^2, Size_{batt}\right) \tag{1.2}$$

Statistical parameters, used to check the quality of the model, show the high correlation of predicted results versus simulation results.

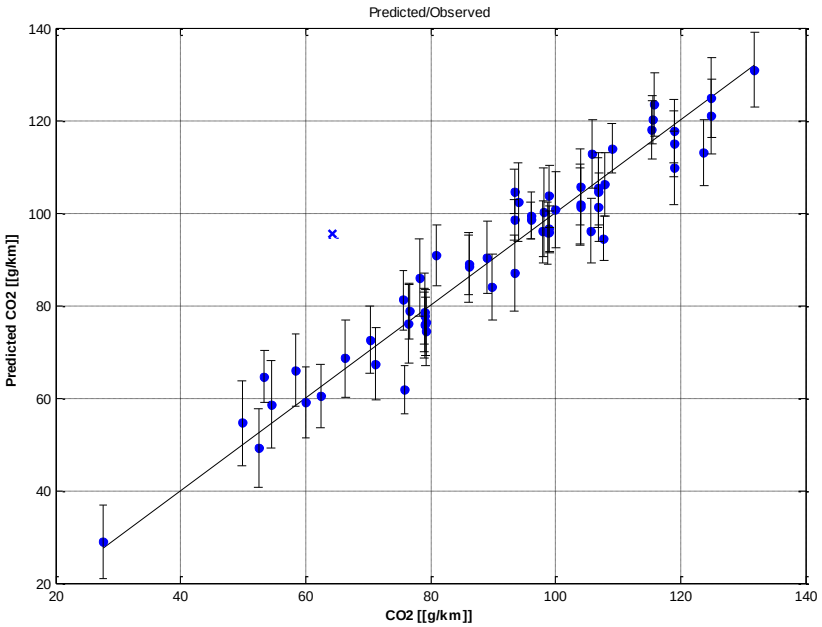

Figura 1.9: Compare of predicted values and observed values of CO_2.

Model	R2	PRESS R2
CO_2	0.937	0.879
Cost	0.981	0.964
Functionality	0.971	0.949
Performance	0.996	0.983
Mass	0.841	0.695
EV Range	0.851	0.739

Tabella 1.8: DoE model results.

1.1.3 Optimization

The hybrid vehicle design methodology uses optimization techniques based on specific algorithms. Once models for design output are defined, a criteria to optimize design parameters is decided.

According to the typology of this study, optimization adopts a MatLab based âf*minconâ* is a function included in MatLab Optimization Toolbox Â© which finds a constrained minimum of a scalar function of several variables starting at an initial estimate. More specifically finds the minimum of a problem specified in 1.3 by

$$min_x f(x) \rightarrow \begin{cases} C(x) \leq 0 \\ c_{eq}(x) = 0 \\ A \cdot x \leq b \\ A_{eq} \cdot x \leq b_{eq} \\ lb \leq x \leq ub \end{cases} \quad (1.3)$$

x, b, b_{eq}, lb, and ub are vectors, A and A_{eq} are matrices, $c(x)$ and $ceq(x)$ are functions that return vectors, and $f(x)$ is a function that returns a scalar. $f(x)$, $c(x)$, and $ceq(x)$ can be nonlinear functions.

As underlined in (7), âthe powertrain system characteristics are highly nonlinear and non-continuous that may have a large number of local optimaâ. The SQP algorithm (9) is an iterative method for nonlinear optimization, that takes every iterative step in the region constrained by bounds. SQP methods are used on problems for which the objective function and the constraints are twice continuously differentiable.

Finally, based on above mentioned algorithms, the optimization is conducted in a specific user-fiendly interface, allowing the user to select target function for optimization, constraints and range of variation for design parameters.

1.2 Power-train design

OEMs, lately, faces the major challenge of designing fuel efficient powertrain which are priced to meet the desired customer value.

In mid to longer term, evolutionary propulsion technologies (Figura1.11) with significant numbers in global vehicle fleet will impact on global fuel consumption and emission reductions. Emerging technologies such as electrification, in combination with optimized ICE have proved that the reductions in fuel consumption and emissions could be attained. However the main challenge today is finding the right mix of technical solutions or design parameters in order to achieve CO_2 reduction and fulfill requirements at minimum cost.

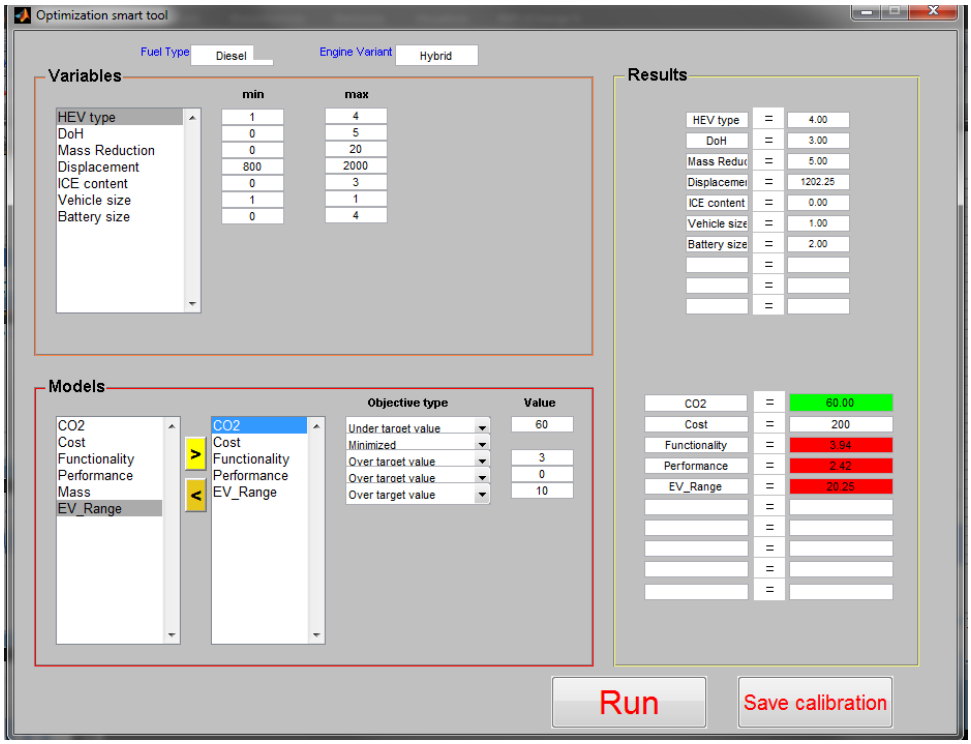

Figura 1.10: The optimization tool interface.

For such matter, an optimization algorythm as presented in **??** is useful to draft scenarios for powertrain development according to predefined targets (i.e. cost, fuel economy).

The methodology, therefore, has been applied to a specific engineering case, to optimize the design of a mid-sized passenger vehicle. The compact vehicle must achieve low fuel consumption over urban driving and must be capable of high fuel economy over extra-urban driving at minimal cost. Therefore, the baseline for the analysis is a conventional diesel powered vehicle.

1.2.1 Battery sizing

Before optimizing the design of the power-train according to requirements, it is important the influence of main design parameters on the design output by using the available model.

The energy size of the battery is one of the major design parameter of the powertrain as it influences the CO_2 emissions, the vehicle mass and it is the most

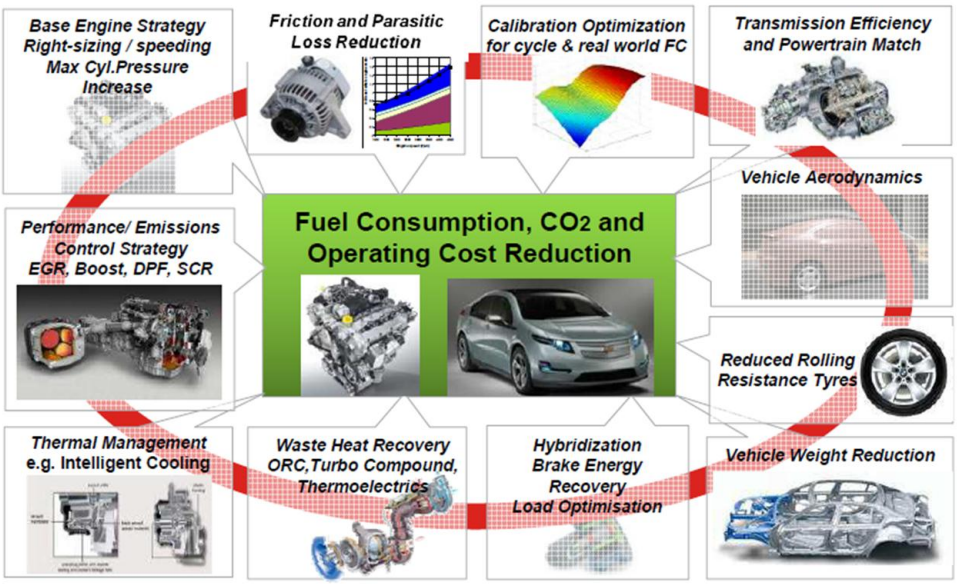

Figura 1.11: Available technical solution to achieve fuel consumption reduction - courtesy of Ricardo: GM workshop May 2012.

cost sensitive. Figura1.12, 1.13, 1.14 reflect results of this analysis.

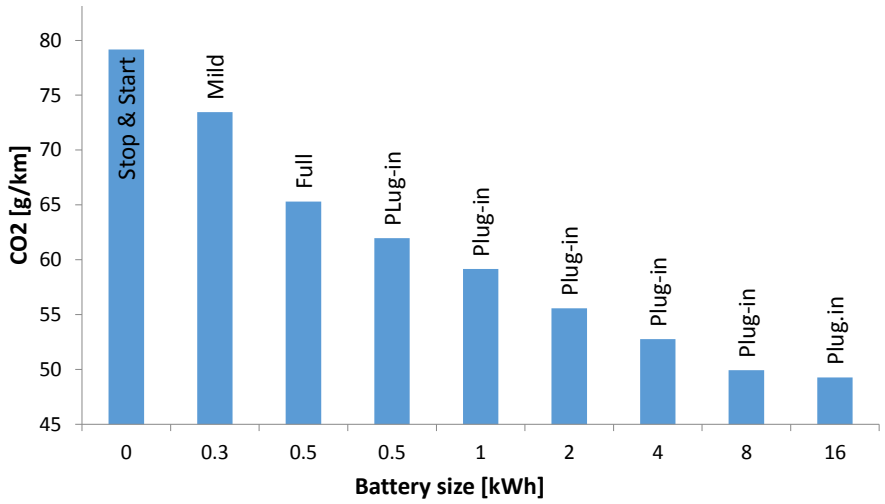

Figura 1.12: Impact of battery size on CO_2 figures.

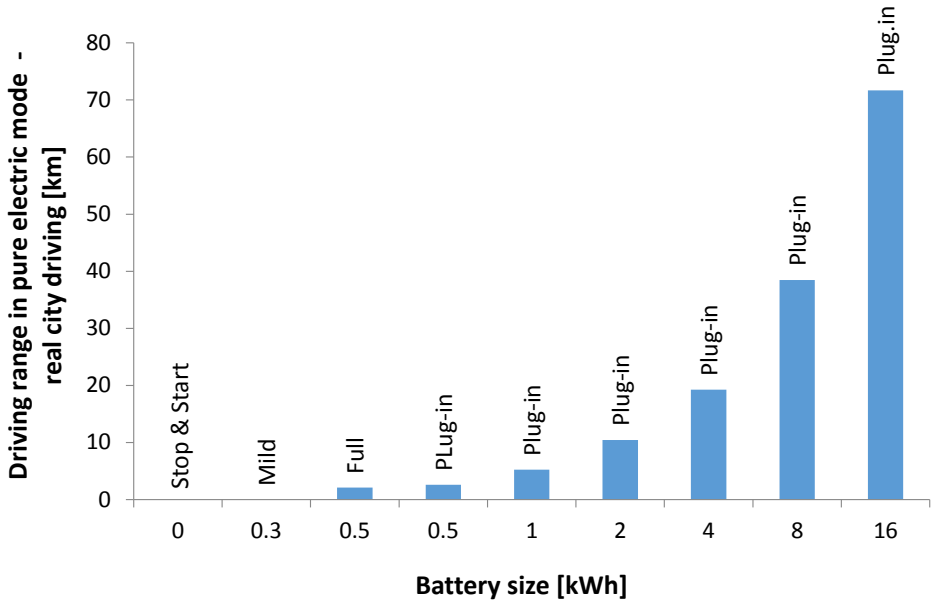

Figura 1.13: Impact of battery size on Pure EV driving..

Overall, the methodology to optimize power-train design performed well. Thus, for early-design stages of the vehicle development process, due to the high spread of technologies and solutions leading to CO_2 reduction, selecting the most convenient path becomes a critical issue.

The adoption of mathematical approach towards optimization of the design at early stages of development, can summarize effects of different technologies and evaluate them on a fair mathematical/statistical base, optimizing towards a selected target.

1.2.2 Power-train evolution scenario

The model developed can be further used to define a technology road map for electrification of diesel engines.

When looking at power-train electrification, two major scenarios might be drafted:

- *Entry-level electrification* applies to technical solution which might offer CO_2 advantages at minimum cost;

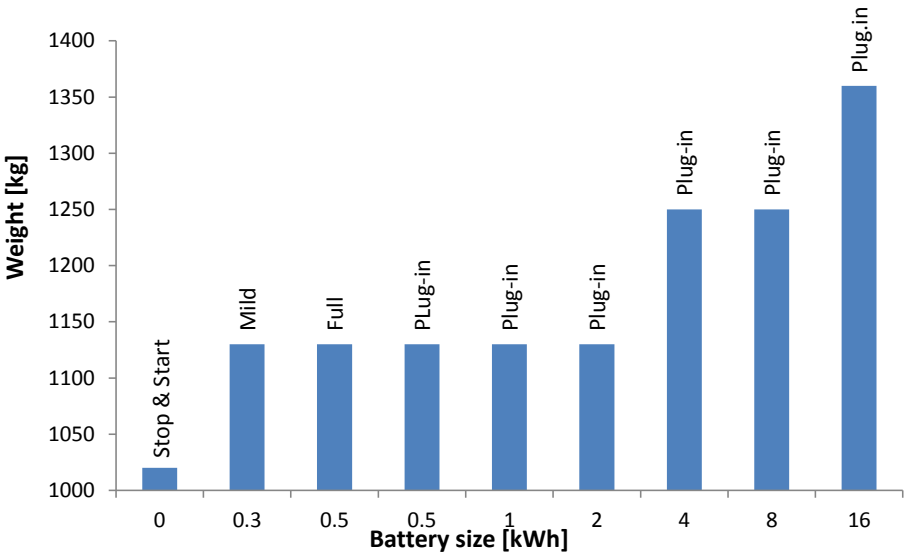

Figura 1.14: Impact of battery size on vehicle mass.

- *High-end electrification* applies to technical solution which might offer significant CO_2 savings and customer features at high cost.

Entry-level electrification An optimized design for entry-level electrification includes a P1 power-train design, having a small electric motor coupled to the engine. A micro-hybrid electrification would be preferred offering a only Stop&Start feature, which shuts the engine off when no traction is required.

High-end electrification An optimized design for high-end electrification includes either a P3 or a P4 power-train design, having a bigger electric motor coupled to the transmission or on the rear axle. A full-hybrid electrification would be preferred offering, additionally to Stop&Start, features a electric boost, energy recovery full electric operation and perhaps All-Wheel-Drive, by running only with the electric motor on the rear axle.

As in Figura1.15, by combining the 2 scenarios a technology road map can be defined, where the diverse technical solutions for electrification are classified by cost and CO_2 saving potential.

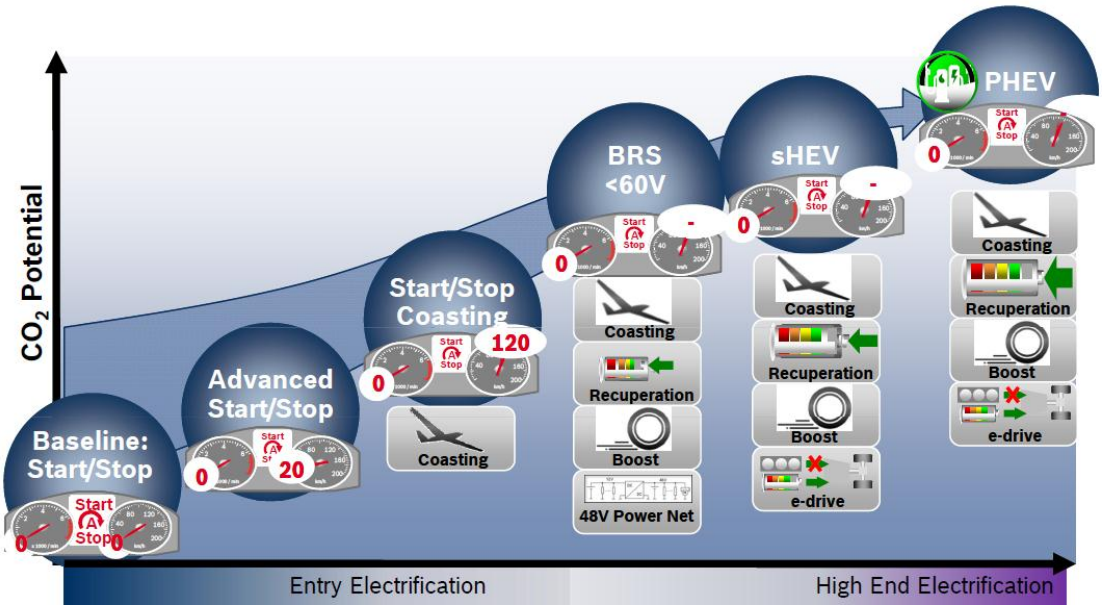

Figura 1.15: Technology road map for electrification of diesel engines.

1.2.3 Architecture selection

In recent years the pursuit of extremely low CO_2 emissions has gathered interest by OEM due to a combination of legislative and market requirements. In particular the European Commission mandate for $95gCO_2/km$ in 2020, as well as a set of market incentives, which favor fuel efficient vehicles, is creating a strong request for technical solutions that may be applied in the OEMs portfolio in order to rapidly impact the fleet overall emission.

Therefore, over the powertrain architecture selected over this study will apply to entry-level electrification scenario, focusing on the development of micro-hybrid vehicles, applying Stop & Start technology.

Other power-train architecture, in order to deploy the additional features, require bigger batteries, which increase significantly the overall cost of the power-train.

Capitolo 2

Enabling sailing for next generation stop & start

Environmental protection and efficient energy utilization have been always important issues in the automotive industry Chapter 1, but have gained significant momentum with the growing demand for mobility around the world and its impact on the global environment. Towards this end, many improvements in automobile technology have been accomplished over the past decades. However, fuel economy with improvements in vehicle, powertrain technology have been penalized by customer preferences. Automotive industry faces the challenge of producing vehicles that meet future fuel economy and emissions requirements which are priced to meet the desired customer value.

As hybrid vehicles, due to the high cost of the electrification they introduce, in next years will not impact the OEM fleet-averaged CO_2 figures in a significant way, it is beneficial to introduce new cost-oriented CO_2 features able to optimize engine operations, as they offer a very favourable cost/benefit ratio.

According to market trend, the increasing interest on automated transmission (i.e. MTA,DCT, e-Clutch) plays a key-role towards the optimization of engine operation. The basic principle of shutting the engine off at idle to remove engineâs drag torque could be adopted at vehicle in motion, extending the distance covered by the vehicle rolling in neutral, when no traction is required, by opening the clutch automatically. Literature calls such operation sailing: represents a low cost control feature, as it does not introduce new components, able to enhance Start & Stop technology.

The paper will assess the impact on fuel economy of opportune strategies to enable sailing both over real world driving and on relevant regulatory schedules. The study will focus on a Diesel engine powertrain, as its higher efficiency than gasoline reduces the space for improvement, it offers greater opportunity by removing

engineâs drag to extend ICE shut-off periods and, due to its higher diffusion in the European market, it impacts CO_2 figures in significantly.

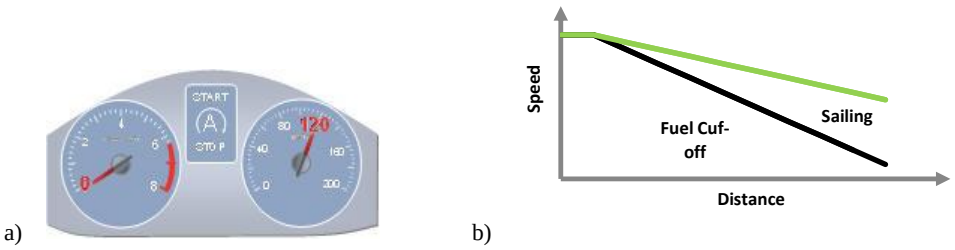

Figura 2.1: a) Engine Stop at vehicle in motion, b) Distance covered by vehicle with std S&S control strategy and vehicle adopting sailing during coasting.

2.1 Stop &Start

Stop & Start technology improves fuel economy by reducing fuel used when the vehicle is stopped, by stopping the engine rotation. It was introduced in Europe in 2008 equipping only a few population of vehicles; in 2012 more than half of vehicles sold in Europe included such system. (17) This growth rate is due to a favourable costbenefit ratio, to improve fuel economy in the New European Driving Cycle (NEDC). Some additional capacity or durability additional components may be added to the powertrain, ie; AGM battery and starter, and Stop & Start mainly requires the development and refinement of controls. Further fuel economy improvement may be possible by extending Stop & Start operation to other vehicle speed ranges.

Though initially Stop & Start technology was primarily introduced in vehicles with manual transmission, this technology has been further developed to be applicable to automated transmissions and show further CO_2 benefit on manual transmission. Today, Start&Stop systems are implemented in all vehicle segments and markets, from entry level up to the luxury segment.

2.1.1 Upcoming regulatory framework

Though, the main assumption behind this scenario is the NEDC cycle adopted for defining fuel economy figures. Such homologation procedure will phase out starting in 2017 through 2020, being replaced by the World Ligh-Duty Test Procedure

(WLTP), impacting, then, the scenario drafted till now.

		NEDC	**WLTP**
Distance	[km]	11.02	23.26
Duration	[s]	1180	1800
Duration of stop phases	[%]	24.8	13.4
Maximum speed	[km/h]	120	131.3
Average speed w/o stops	[km/h]	44.6	53.8
Average speed w/ stops	[km/h]	43.6	46.5
Minimum acceleration	[m/s2]	3.80	6.00
Maximum acceleration	[m/s2]	−5.00	−5.40
Average acceleration	[m/s2]	2.14	1.46
Average deceleration	[m/s2]	−2.84	−1.6
Energy required over cycle	[kWh]	1.25	2.44
Average energy over cycle	[Wh/km]	114	105

Tabella 2.1: Key parameters of the NEDC, WLTP

In 2.1 the key parameters of both cycles are reported in order to compare NEDC and WLTP. While in NEDC the vehicle spends almost a quarter of the time at idle, over WLTP the vehicle is stopped only for about 13% of the time, impacting, then, fuel economy benefit of Stop & Start technology as it is intended today. Although WLTP cycle shows stronger acceleration, deceleration than NEDC, the average values of acceleration, deceleration of WLTP are lower than NEDC (16). As a matter of facts, several phases over WLTP are characterized by smooth deceleration profiles Figure 2 b) below the $1m/s^2$. Indeed, over NEDC, decelerations occurs less frequently and show steeper profiles.

2.1.2 Evolution of Stop & Start Technology

The basic principle of Stop & Start technology is the elimination of engine drag torque at idling conditions, i.e. when propulsion is not required (i.e. at vehicle stop). We will refer to Conventional Stop & Start in the following.By turning off the combustion engine when decoupled from the drivetrain, the fuel that is injected simply to overcome the combustion engine friction, is saved. A similar concept can be applied in order to improve fuel economy at higher vehicle speeds. Nowadays, almost on every vehicle all engine are equipped with smart engine controls as DFCO which turns off fuel injection as soon as the driver releases the gas pedal. Though, during DFCO, engine is driven by the vehicle, its friction and pump losses cause a significant loss of energy. Depending on the engine size, type and design, the motoring torque and therefore the resulting motoring power can be significant. Figura2.3 reports

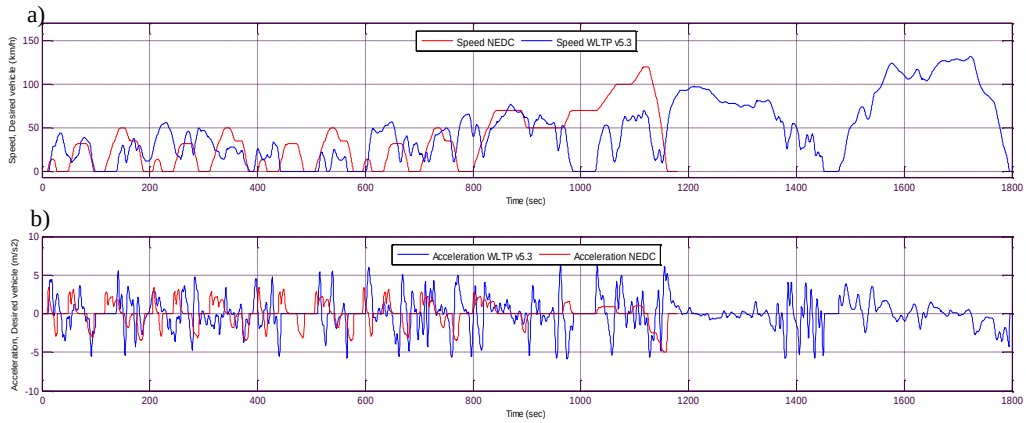

Figura 2.2: Speed (a), acceleration (b) profiles of NEDC and WLTP

typical values of engine fmep (friction mean effective torque) for turbocharged light-duty diesel engine, depending on engine speed. The engine speed in a vehicle depends on vehicle speed and the gear/transmission ratio.

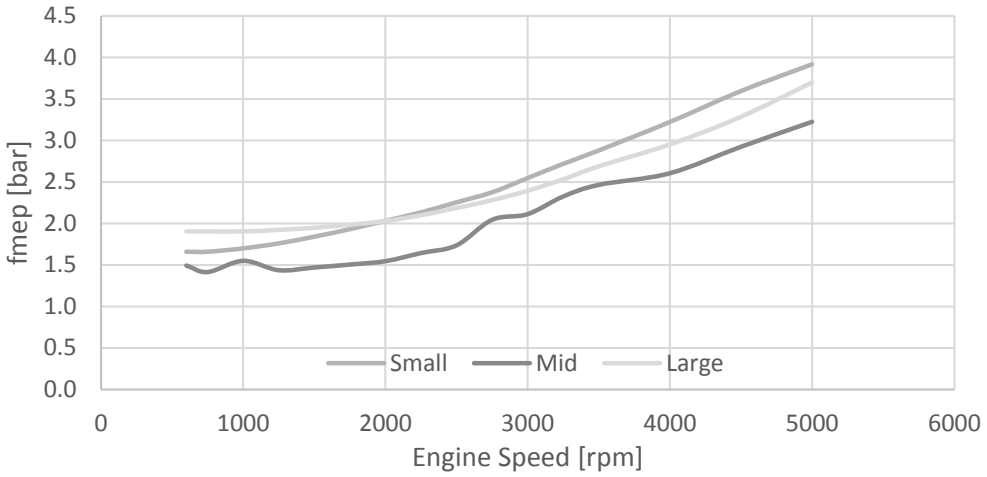

Figura 2.3: Engine fmep for different sizes of conventional light duty turbocharged diesels.

The fuel consumption benefit provided by Stop & Start lately has been further enhanced extending its range of applicability on cycle. Conventional Stop & Start

system enables engine shut-off when vehicle is shifted into neutral at a stop. Due to homologation procedures, such operation provides fuel economy improvements on NEDC (2.4).

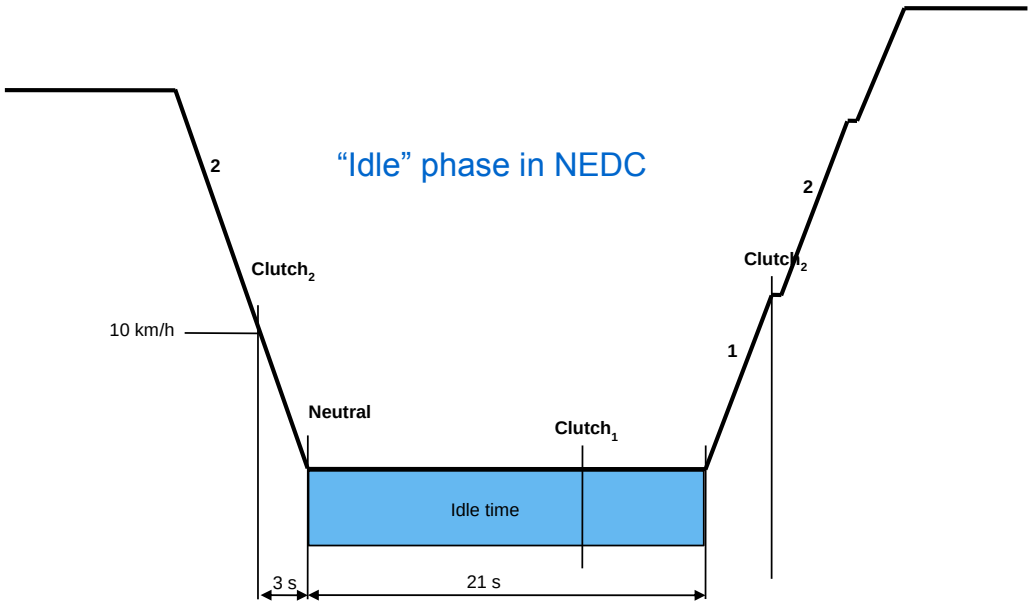

Figura 2.4: Fuel economy opportunity during idle phases over NEDC

Although the energy required to motor the engine varies according to the vehicle mission, the fuel engine propels its amount is significant only might be quite significant. Though, over the cycle the fuel provided is spent for more than 22% to motor the engine (2.5).

To remove the engine motoring torque during coasting, a free-wheel overrunning one-way clutch (OWC) may be included into the vehicle's transmission, allowing the transfer of positive torque only. A OWC adds complexity of a second controlled bypassing clutch, for use during down-hill driving, when the brake effect given by the essential combustion engine's motoring torque is required. A similar effect could be achieved via ârolling in neutralâ: by opening the clutch or by shifting the transmission into neutral the engine is decoupled from the drivetrain whenever the driver requires a negative torque. Literature (17) (18) defines the effect of extending the distance covered by the vehicle freewheeling, when no traction is required, by opening the clutch automatically and removing engineâs drag torque, as âSailingâ. We will refer to âSailingâ in the following.

As a matter of facts, the driver can experience Sailing by an increased coasting distance, which is illustrated in 2.6: a C-segment vehicle equipped with a mid-sized

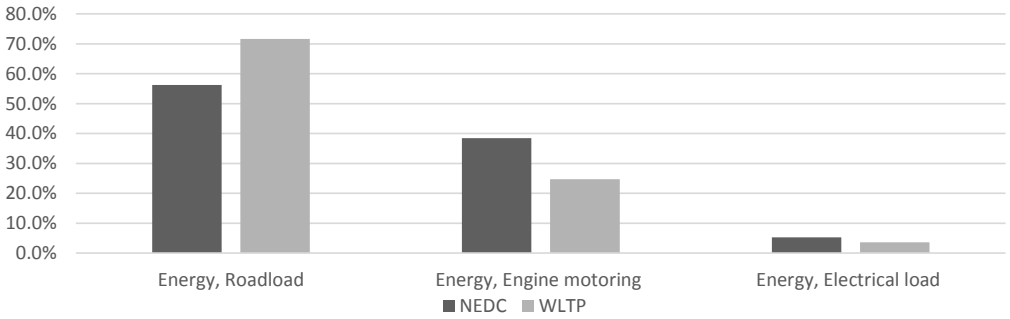

Figura 2.5: Analysis of energy spent over cycle to propel the vehicle, motor the engine, charge the electrical system.

diesel engine can sail for a distance more than 30% in comparison to coasting in 6^{th} gear, starting at 120 km/h.

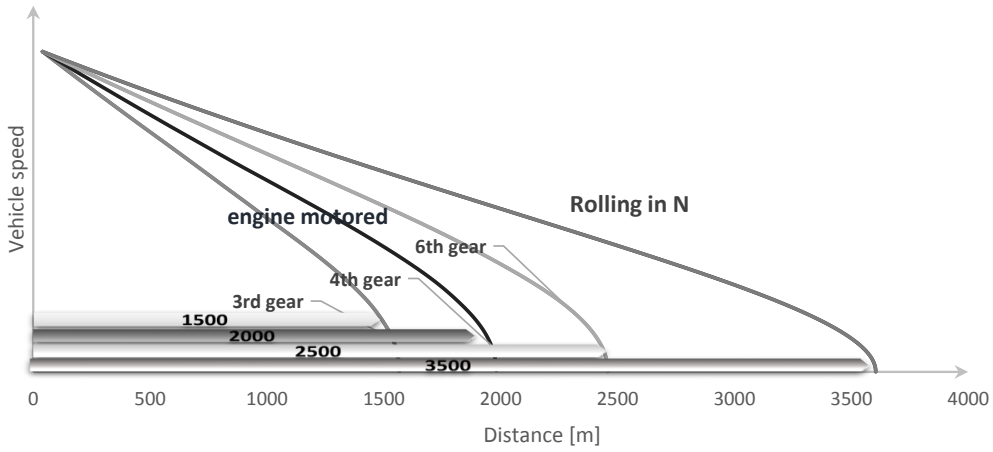

Figura 2.6: Coasting distance covered by a mid-sized vehicle in different gears and by rolling in neutral.

Opening the clutch under such sailing conditions gives the options either to turn off the combustion engine or to operate it at idle speed: we will refer to as Stop & Start Sailing and as Idle Sailing, respectively. Therefore, the potential improvement in fuel economy by adopting Sailing could be significant. Indeed, fuel consumption at idle can still be beneficial in comparison to a minimal fuel injection that only

compensates drag losses. Though, the fuel economy potential of Sailing depends strongly on the speed profile, i.e. driving cycle. For vehicle certification purpose, this speed profile is defined by legislation (like WLTP or NEDC emission test cycles). This study assess the potential fuel economy improvement of Stop & Start Sailing in comparison to available Stop Start system for upcoming homologation speed profile.

2.2 Sailing

A possible operating concept for sailing is presented, which could be implemented regardless of the transmission type: i.e. such approach is feasible with any automatic transmission (DCT, MTA, AT) and manual transmission with automated clutch. Idle Sailing can already be activated by a driver today. For a vehicle with manual transmission, the driver could simply depress the clutch pedal, or shift into neutral gear. Shifting from âDâ to âNâ would do the same task in vehicle with automatic transmission. S&S Sailing, then, could be implemented and operated in a similar manner like a Start& Stop function. Though, such approach would require a significant effort to the driver and change in his driving style.

Indeed, an automatic control would activate sailing according to the torque requested by the driver by pressing either the accelerator or the brake pedal. The torque request, then, according to the vehicle speed, corresponds to a specific acceleration/deceleration. Figura2.7 compares the deceleration performed by the vehicle in neutral and in gear. By activating sailing automatically, vehicle will decelerate as in neutral (red line) when driver will release pedals and will be able of controlling the vehicle deceleration by means of the brake pedal, having the driveline disengaged. If the deceleration requested via brake pedal will be lower than what could be achieved by coasting in gear, then vehicle will exit sailing and perform DFCO. Such activation of sailing would be beneficial as for small accelerator pedal pressure the injected fuel does not produce any positive torque at the engine crank shaft, rather compensates the engine drag torque. Sailing would, indeed, avoid such fuel consumption.

2.2.1 Simulation tool

Sailing control was implemented in a 1D, time based, lumped parameter dynamic simulation of the vehicle system. Longitudinal motion of the vehicle and rotation of the engine, transmission and driveline are modeled. The GM proprietary vehicle energy model has been an effective tool for studying the fuel economy of various vehicle configurations, due in large part to its modular swappable design. The simulation tool is developed in the Matlab / Simulink / Stateflow environment. This

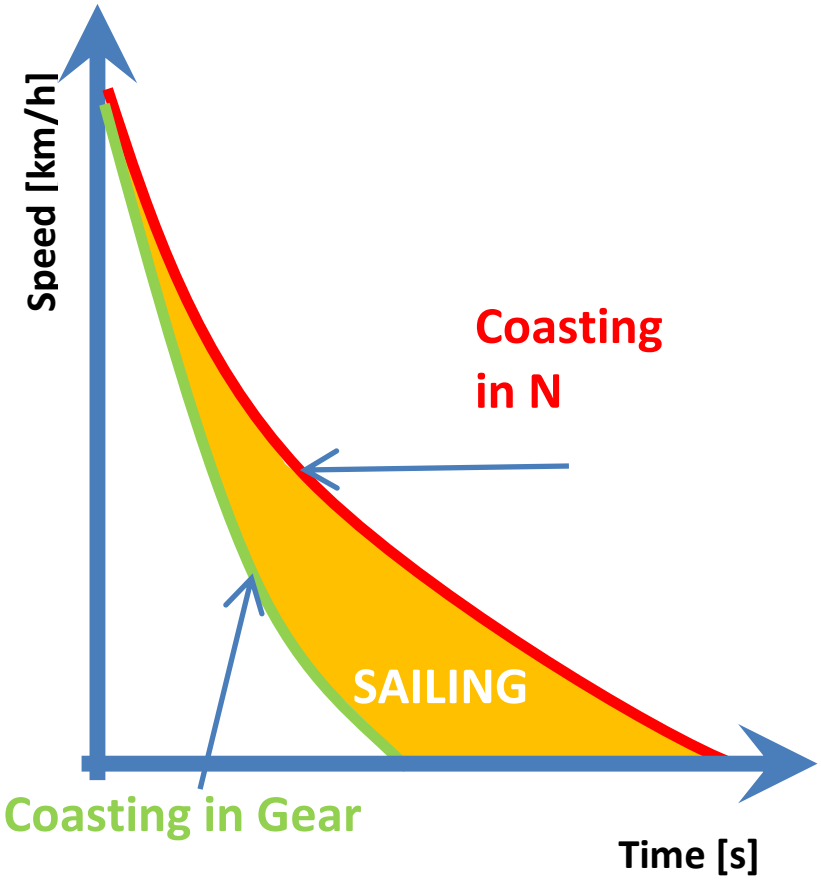

Figura 2.7: Sailing opportunity on vehicle

model uses Simulink and custom libraries to define the behaviour of the powertrain, driver and vehicle. The model is organized into subsystems that include a driver, a vehicle model and a powertrain model. The powertrain is further broken into component models that mirror physical components such as the engine, transmission, accessories and batteries. Supervisory control functions are modelled using a combination of Simulink and Stateflow. Experienced users can add, modify and improve functions in the model. The ability to modify the model is especially important for control and calibration optimizations. The vehicle driver model is a closed-loop model of a human driver. The driver model controls the simulated vehicle speed to follow the desired trace according to the mission, within a specified error tolerance. The driver model uses acceleration pedal position and vehicle braking command as control inputs to the vehicle and powertrain model. The simulation tool can

perform computation within minutes for WLTP fuel economy cycle. The inclusion of the Sailing model into UM is done following the modular construction of the simulation tool so that the control strategy can be used to study other platform combinations as well. Engine usage, energy distributions and fuel economy figures are shown based on simulation results.

2.2.2 Simulation results

All the simulation work has been conducted on C-segment vehicle equipped with a mid-sized turbocharged diesel engine and manual transmission.

Although fuel economy drivers might achieve significant fuel economy drivers might alternate light acceleration at sailing phases, such function might not be tolerated by average drivers. The CO_2 reduction potential of Sailing depends on driving cycle. Since the vehicle speed profile during Sailing operation depends on many vehicle parameters, e.g. tires, aerodynamics of car body, vehicle mass and external factors like road grade, any predefined speed profile with a limited speed tolerance band inherently limits the benefit of Sailing. Though, the CO_2 reduction benefit of Sailing can be foreseen by evaluating the key parameters of cycles and closely analyze speed profile.

In section âUpcoming regulatory frameworkâ, the average deceleration over cycle reported lower values for WLTP than NEDC. In facts, while the NEDC consists of many steep deceleration phases which can be perfectly achieved in DFCO, WLTP shows frequent smooth decelerations which could not be achieved if coasting in gear and would perfectly fit with Sailing.

In section **??**, the average deceleration over cycle reported lower values for WLTP than NEDC. In facts, while the NEDC consists of many steep deceleration phases which can be perfectly achieved in DFCO, WLTP shows frequent smooth decelerations which could not be achieved if coasting in gear and would perfectly fit with Sailing.

During driving, engine power is mainly used to compensate vehicle road load (i.e. aerodynamic drag, rolling resistance and inertia) and to motor the engine. Even though there are frequent smooth deceleration on WLTP, a positive engine power is detected, which corresponds to the engine motoring power. In Figura2.8 sailing events can be easily detected when the engine brake power is between the road load power and engine motoring power.

Figura2.9, then, reports the opportunity for sailing events over the whole sailing in comparison with DFCO phases, when the driver is requested to press the brake pedal.

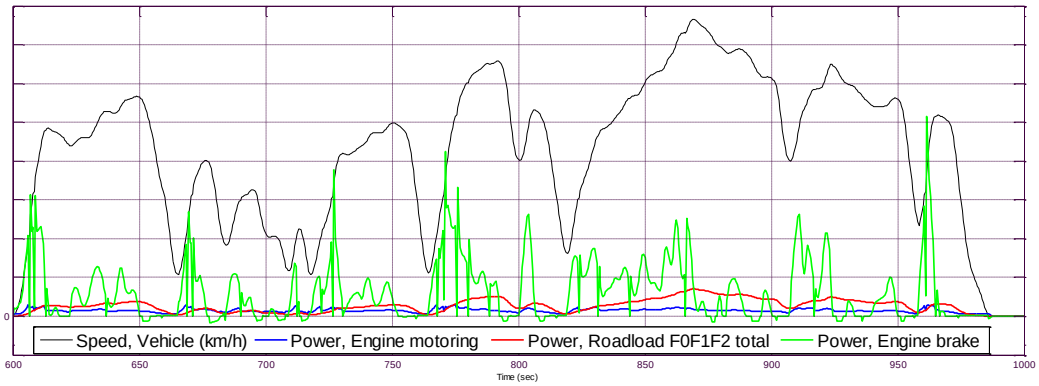

Figura 2.8: Power request over mid-segment of WLTP

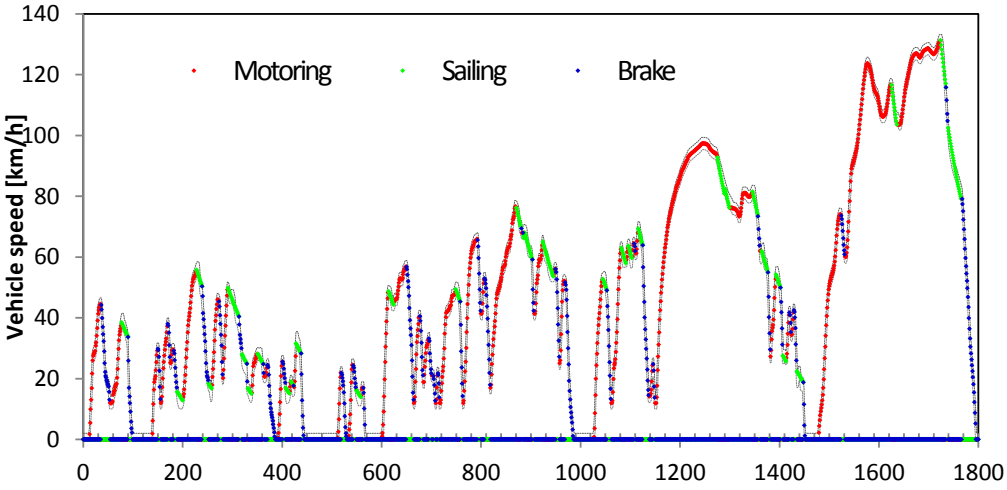

Figura 2.9: Sailing events over WLTP

2.2.3 CO_2 figures

The fuel economy benefit of Stop & Start varies according to vehicle mission and, though, to the homologation cycle. Moving from the NEDC to WLTP, the time spent at idle is reduced by half. Therefore conventional S&S system will also be reduced by half, moving from the NEDC to the WLTP. Further enhancement, as Extended Stop & Start, which could be implemented by a dual-solenoid stater for a quicker engine restart, shows a positive fuel economy benefit on NEDC, while it loses much of its potential when moving to WLTP. Therefore, in order to maintain the fuel benefit of Stop & Start, engine should be stopped in other phases over WLTP.

Sailing seems the right fit for the upcoming regulation, enhancing the benefit of S&S by an additional 3.5%, as per Figura**??**. Such feature could be easily implemented on automated transmissions, it could be implemented on manual transmission by introducing electrically actuated clutch system.

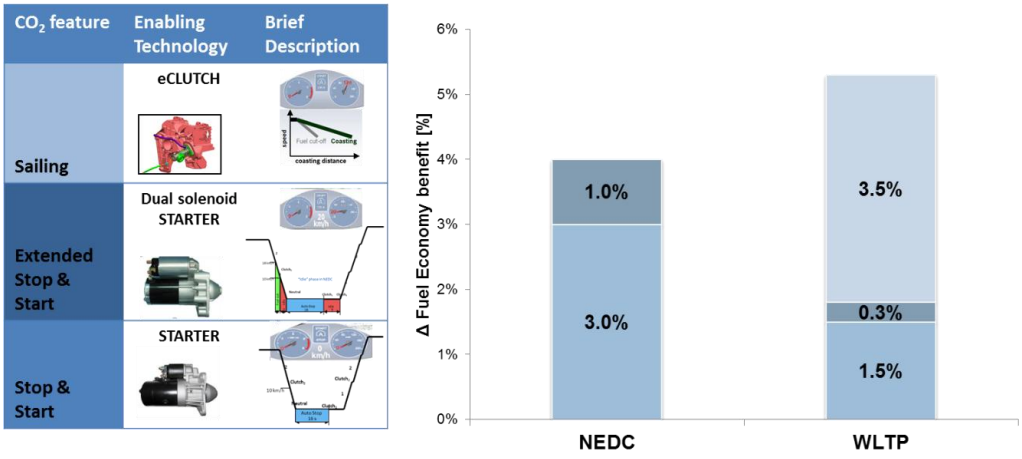

Figura 2.10: Fuel Economy scenario of Stop & Start technology over NEDC and WLTP

Idle sailing has not been further evaluated in this study as its fuel economy potential over WTLP is not significant. Tabella2.2 reports fuel economy figures in comparison to an S&S vehicle

	WLTP
S&S Sailing	−3.5%
Idle Sailing	−0.3%

Tabella 2.2: Fuel economy figures of idle sailing vs. S&S sailing

The change in the homologation procedures transition from NEDC to WLTP will impact significantly the fuel economy potential of todayâs Stop & Start, losing half of its benefit. Therefore, in order to maintain its favorable cost/benefit ratio such technology must extend its usage at higher engine speed. Sailing, though, represents the next logical step in developing Stop & Start technology, eliminating the combustion engine's drag torque.

Moreover, as such feature reports even higher fuel economy improvements than on cycle, by increasing the distance covered without fuel injection, it might be

helpful to close the gap between publicized and real fuel consumption of vehicles, which corresponds today to a major complain by customers.

2.3 System Requirements

Although S&S Sailing requires integration efforts on all vehicleâs subsystems, idle sailing does not provide significant fuel economy benefit to be used on cycle. Strategies activating sailing automatically and stopping the engine without any operation required to the driver will be essential for its introduction, in order to gain fuel saving if operating it on cycle. Turning off the combustion engine during coasting conditions increases the number of engine starts over vehicle lifetime, impacting starter system, vehicle power net, steering, bracking, trasmission and HMI.

Though, Stop & Start technology affects primarily starter motors. Today they are typically designed for Start&Stop applications for up to 300.000 engine crank over vehicle lifetime. This number can double for Start&Stop Sailing applications. Therefore, a new solution to crank the engine must be applied, as performing engine start via clutch closure. We will refer to 'Clutch Assisted Start' in the following. The automation of transmission as MTA, DCT and by introducing a clutch-by-wire system for manual transmission vehicles, paves the way in introducing such new operations. As a matter of facts, the number of load cycles for the starter motor can be reduced significantly if the engine is revved up via clutch. An appropriate clutch control strategy allows to comfortably rev up the combustion engine above approximately $50 km/h$. Nevertheless a significant increase of the starter motorâs load cycles will remain.

Moreover, Short engine start times are of utmost importance for Start&Stop Sailing applications. They are especially challenging if an engine restart is requested already during engine run-down, i.e. during so-called Change-of-Mind (CoM)[1] situations. Clutch Assisted Start reduces the tip-in delay in such phases, by tamping up the engine faster.

The following chapters focuses on the development clutch assisted start by applying a new methodology based on modeling and simulation.

[1] Change-of-Mind (CoM) situations occur, if the engine is about to be turned off, when all of a sudden an engine start request occurs because the driver wishes to accelerate. This is more common for automatic transmissions, when the driver steps on the brake pedal (triggering an engine stop) and releases the brake pedal shortly after (triggering an engine restart). Typically, engine start times are longer at such situations since current pinion gear starter motors cannot engage at higher engine speeds, meaning that the starter motor can be actuated only after the engine has completely stopped rotating. This application specific lag time of up to more than 1 second affects the driver more for Free-Wheeling applications, since vehicle response during driving is more essential than during standstill.

Capitolo 3

Modeling of the vehicle driveline

Starting the engine through clutch engagement consists in spending a certain amount of the traveling vehicle kinetic energy to spin up the engine. Clutch assisted start, though, will cause the vehicle to decelerate and it will introduce a jerky behavior in the drive line leading to discomfort for passengers: an appropriate clutch closing strategy can mitigate such effect.

Hence, a torsional model of the driveline allow to investigate the impact on drivability for different clutch engagement in different operating conditions in order to fulfill drivability requirements.

A full driveline model, from engine to wheel, has been developed in AMESim[1]aims to analyze the dynamic behavior of the powertrain component.

In this chapter the modeling in AMESim of the driveline and of its components will be explained. The vehicle architecture considered refers to a conventional front wheel drive vehicle equipped with manual transmission. The overall system (Figura3.1) is composed of the following main elements:

[1]AMESim stands for Advanced Modeling Environment for performing Simulations of engineering systems. It is based on an intuitive graphical interface in which the system is displayed throughout the simulation process. UsingÂ AMESimÂ you build sketches of engineering systems by adding symbols or icons to a drawing area. When the sketch is complete, a simulation of the system proceeds in the following stages:

- Mathematical descriptions of components are associated with the icons;
- The features of the components are set;
- A simulation run is initiated;
- Graphs are plotted to interpret the system behavior.

- *Engine*: a 4 cylinder light-duty passenger car diesel engine, modeled in order to compute torque resulting on crankshaft from in-cylinder gas pressure wave and contrasting frictions.
- *Starter motor*: electric starter meshing with the flywheel ring, torque vs. speed command.
- *Dual Mass Flywheel (DMF)*: flywheel designed as a dynamic torsional absorver, composed by two masses, supported by a springdamping system, reducing engine pulsation transmitted to gearbox.
- *Clutch*: actuated by an onoff control, transmitting the portion of torque according to his position.
- *Gearbox*: a manual transmission with non-infinite stiffness of the shafts and ideal efficiency ($\eta = 1$).
- *Differential*: ideal bevel mechanism with fixed ratio driving a standard differential ($50\% - 50\%$ torque distribution).
- *Axel shafts*: with non-infinite stiffness.
- *Wheels and tires*: wheels are modeled as rotating inertias and tires are described by torsional stiffness and damping ideally without slip with the ground.
- *Vehicle*: considered as a translating mass and resistant force, calculated by coast-down parameters.

3.1 Engine starting system

The starting system consists mainly of a starter motor which meshes with the flywheel and provides enough torque for the engine to win initial frictions and inertias, reaching the firing condition Figura3.2.

The complete system model is the assembly of the components involved, considered as sub-models:

- Starter motor
- Flywheel
- Engine

The AMESim modeling of the starting system is presented in Figura3.3

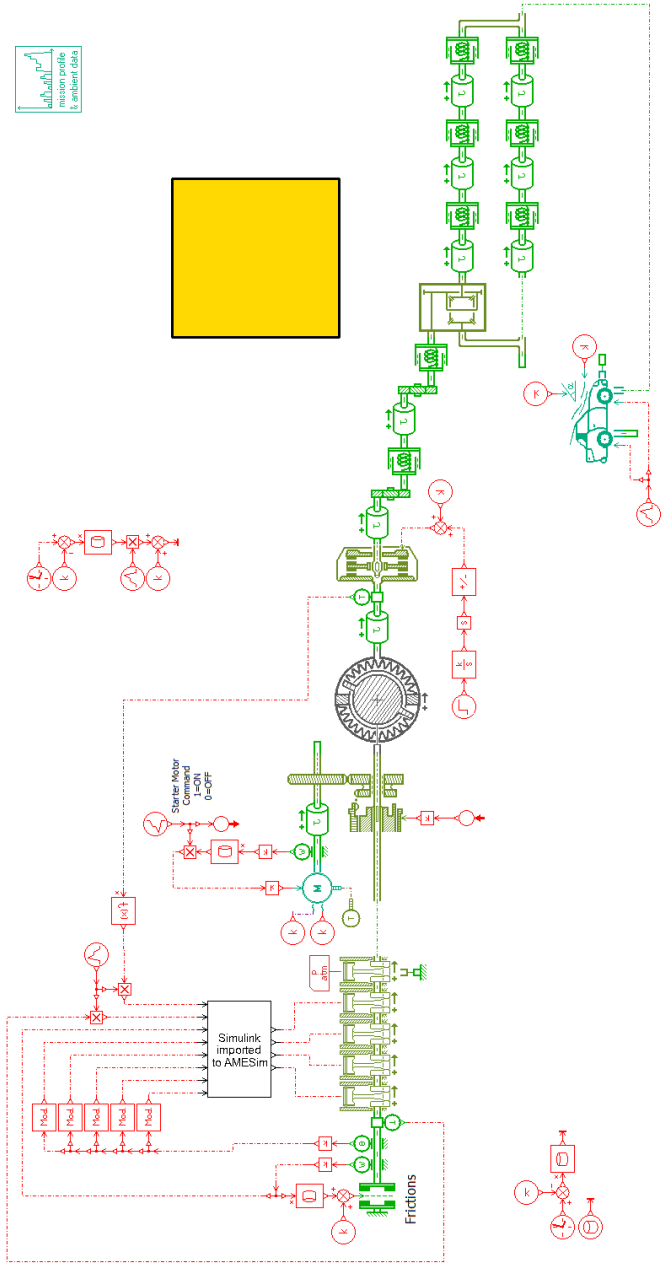

Figura 3.1: The AMESim model of the powertrain and driveline

3.1.1 Starter motor

The torque command is achieved from the starter performance table. This table is available in the starter datasheet and provides the values of torque delivered by the

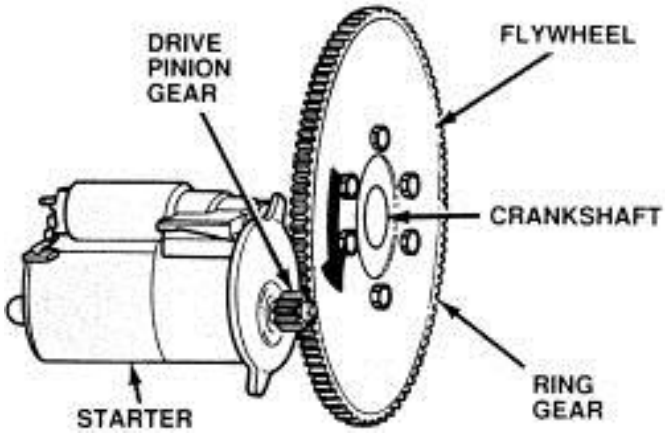

Figura 3.2: Starting system schematic

motor as a function of the shaft rotary speed. The starter characteristic is plotted in Figura3.5.

Thus the control system for the starter is a closed loop control in which the actual velocity of the shaft is read and the torque command is given by interpolating the performance table data. To simulate the duration of the starter action, a 0-1 (OFF-ON) time based signal is multiplied to the torque command. The control system is presented in Figura3.6 and the flow of information is schematized.

The starter motor torque is delivered to the pinion, modeled by its inertia and a gear (pitch radius available in the datasheet), which meshes with the teeth of the flywheel ring. In order to simulate the solenoid action, which pushes the gear to mesh, a synchronizer coupled with an idle gear simulates the engagement and disengagement. It is directly controlled by the $0-1$ starter motor command. A viscous friction coefficient was considered for approximating losses in bearings and other components inside the starter. To improve the model, contact losses between the teeth and backlash effect could be taken into account, considering non ideal contact stiffness, damping and clearance.

3.1.2 Dual Mass Flywheel

It consists of a primary mass and a secondary mass connected to each other via a spring/damper system and supported by a deep groove ball bearing so they can

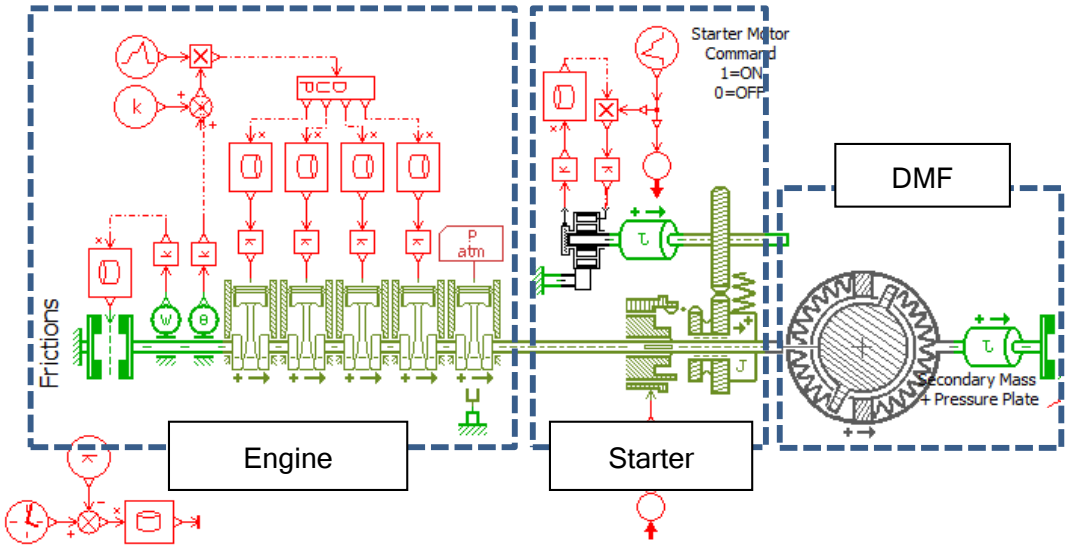

Figura 3.3: Engine and starter motor modeling in AMESim

rotate against each other. The primary mass with starter ring gear is driven by the engine and tightly bolted to the crankshaft.

The DMF is modeled (Figura3.8) considering its main components:

- **The primary mass** (on the engine side) that is rigidly connected to the crankshaft. It is considered in the overall engine inertia;
- **The secondary mass** (on the transmission side) that is the element on which the clutch disc engages, coupling the transmission with the engine. It is considered as a single body with the attached pressure plate of the clutch.
- **The elastic elements** between the two masses are a set of springs and dampers that determine the torsional stiffness of the DMF and therefore its vibrational behavior.

The ring gear, that meshes with the starter pinion, is added into the primary side and has the aim to deliver the torque from the starter to the crankshaft with the correct gear ratio, determined by the flywheel working pitch radius. The synchronizer of the starter motor engages and disengages the pinion from the ring gear.

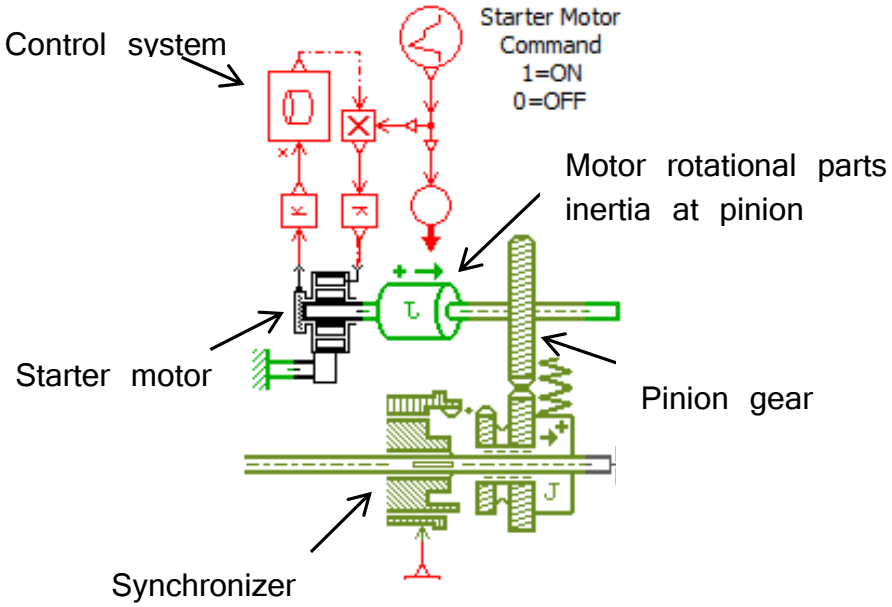

Figura 3.4: Starter motor AMESim modeling

Hysteretic components of elastic dampers and internal frictions are also considered and modeled as rotary frictions that dissipate energy. This kind of flywheel, especially in diesel engines, allows to dump down transmitted vibration to the driveline (3.9) and improves gear change quality.

The advantage in terms of fluctuation reduction achievable from the Dual-Mass Flywheel can be observed through a comparison between the angular velocity of the crankshaft (linked to the primary mass) and the resulting angular velocity of the secondary mass of the flywheel. The plot in Figura3.10 shows this comparison when the engine is in idle condition. The reduction of fluctuations is remarkable, leading to noise and vibration reduction and therefore better comfort.

Moreover, by operating as a dynamic torsional absorber, the system moves the resonance speed range at very low values, ensuring excellent damping of engine vibration even at idle speed. In Figura3.11 it is shown a comparison of the frequency domain, related to engine velocity, of conventional powertrain with torsional absorber clutch disk and powertrain with DMF.

On the other hand this results in worst performance during engine cranking

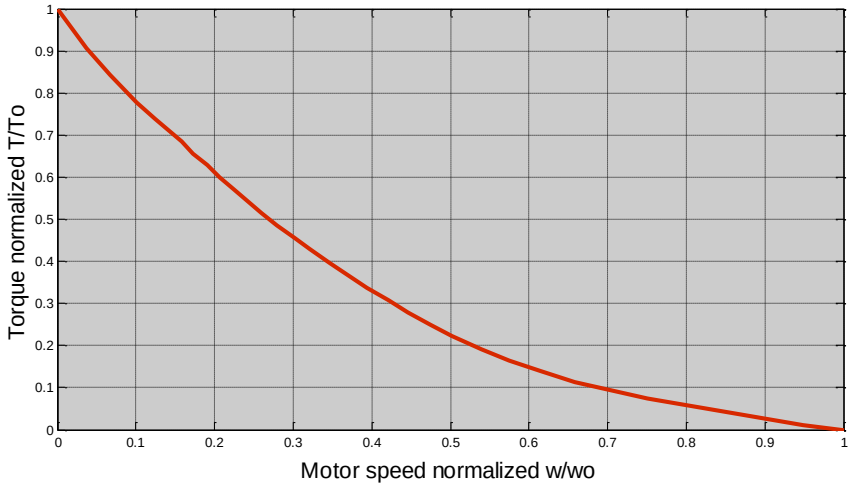

Figura 3.5: Starter motor characteristic curve: Torque vs. Speed

phase, as DMF shows a peak of frequency at low crankshaft speed. When the engine is started the DMF vibration speed range is crossed. For frequent engine starts, required for example by Start/Stop system, such event can lead to DMF failure over time. The DMF model used for this work has a two-stage spring and damper system. During the first stage load is applied only on the softer springs, while in the higher torque ranges, load is exerted by the springs with higher stiffness (second stage). The characteristic of the system is shown in (Figura3.12). Because of internal frictions and hysteresis of damping elements, the characteristic shows a loop in the response of the system.

Then, in order to verify AMESim model of DMF, it must replicate characteristic torque curve. The AMESim model is tested locking the secondary mass of the DMF while an increasing and decreasing torque is applied on the primary side. The resulting characteristic plot of the torque vs. relative angular displacement is presented in Figura3.13. The torque is normalized by a nominal maximum torque $T0$. The result validates the model.

In order to find the vibrational modes of the DMF [2] during its two operating

[2]AMESim main tools for linear analysis are fast Fourier transform (FTT), Eigenvalues calculation for different conditions of the system, modal shapes analysis, plot of Bode, Nichols, Nyquist diagrams and of root loci.

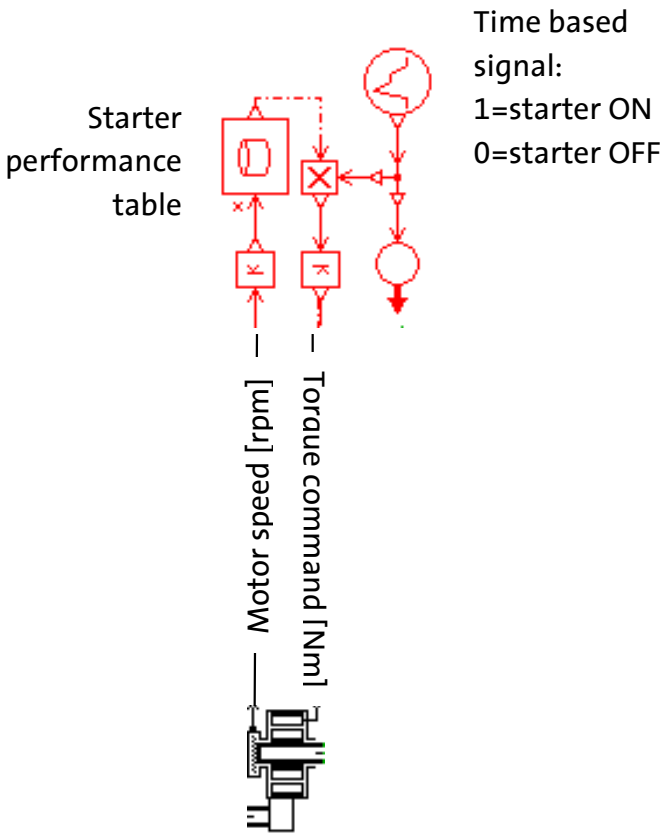

Figura 3.6: Starter motor control system

stages the case in which it is not coupled with the driveline is considered first. To induce oscillations between the two sides of the DMF, a rising and decreasing torque with a ramp function is applied on the primary side (engine side) so that to bring the DMF in both operational stages (Figura3.14). In Figura?? it is shown the response to the ramp function. The variation of the velocity between the two sides indicates the main mode of vibration of the DMF.

From the analysis, the vibration frequencies of the DMF, when working in the first and second stage, are detectable. The frequency value when the flywheel is subjected to an increasing torque is slightly higher than with a decreasing torque. This is mainly due to damping components subjected to hysteresis and frictions of sliding parts inside the DMF (as it can be seen from the DMF characteristic chart in Figura3.13)

Figura 3.7: Schematic representation of Dual Mass Flywheel

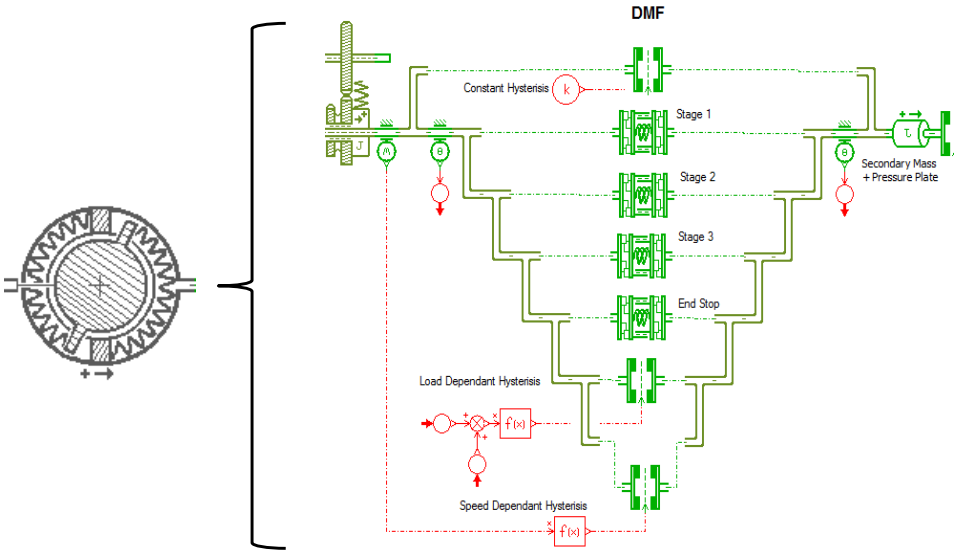

Figura 3.8: AMESim model of DMF.

The Bode diagram gives a more detailed description of the frequency response of the DMF system. Setting the input torque to the primary side as a control variable,

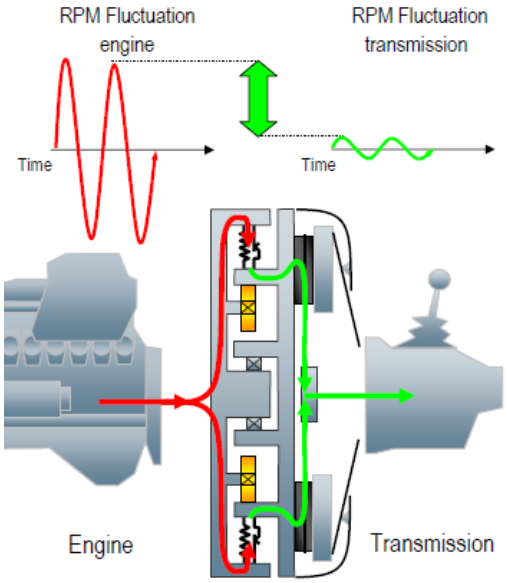

Figura 3.9: DMF fluctuation reduction schematic.

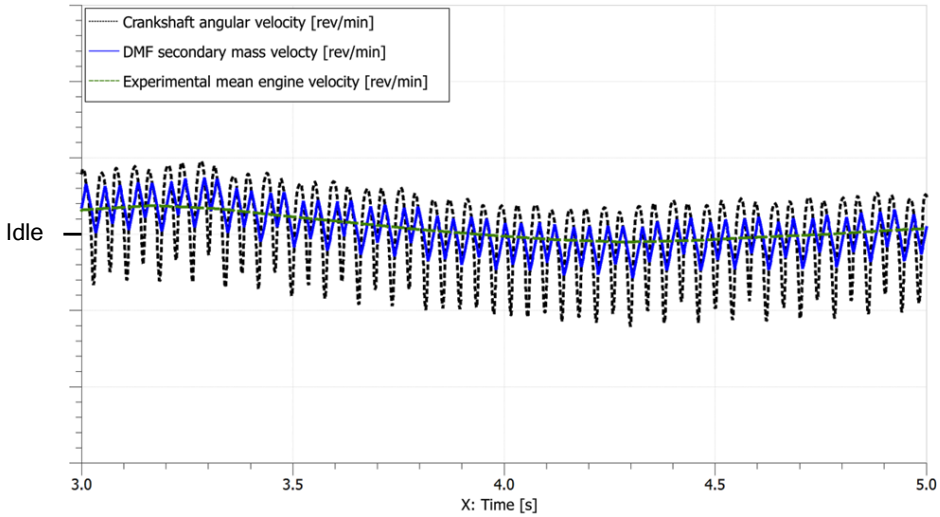

Figura 3.10: Comparison between crankshaft velocity and secondary mass velocity.

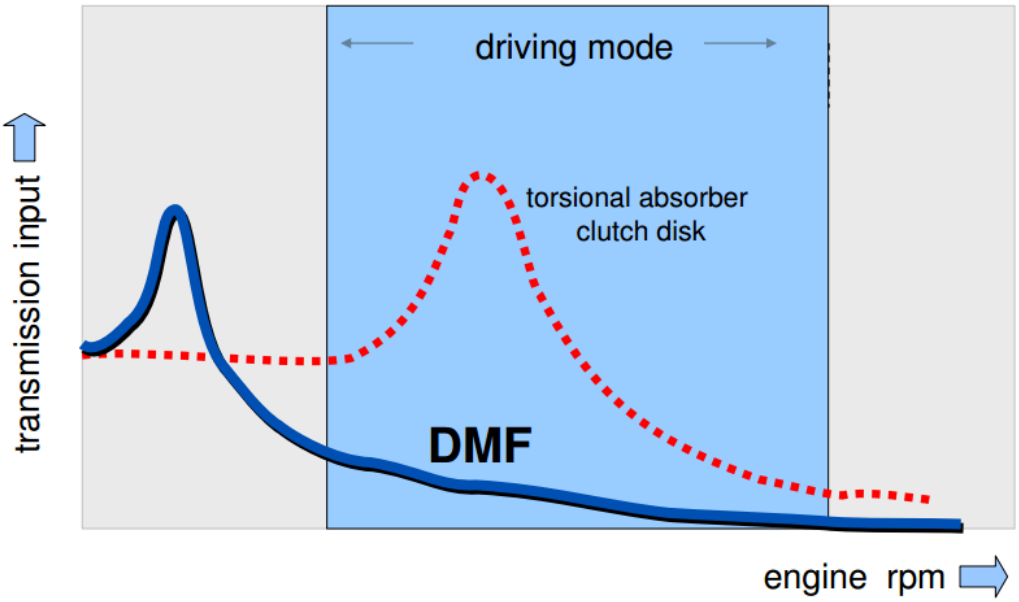

Figura 3.11: Frequency domain of DMF compared to a torsional absorber clutch disk.

the diagrams of gain and phase variation with frequency are plotted for the output torque to the secondary mass of DMF. For both operating stages the Bode diagrams are plotted in Figura3.16, Figura3.17.

The maximum amplification values occurs of course at the frequencies of vibration previously seen in Figura3.15. Once the response in the frequency domain is achieved, it can be defined also the vibrational behavior of the DMF with the engine speed. As described in the introduction part of this chapter, the main fluctuation frequency of the crankshaft speed can be computed as:

$$f_n = \frac{(n[rpm])}{60 \cdot 2} \tag{3.1}$$

Therefore the engine speed n expressed in [rpm] that introduces these frequencies can be easily obtained:

$$n[rpm] = \frac{f_n}{2} \cdot 60 \tag{3.2}$$

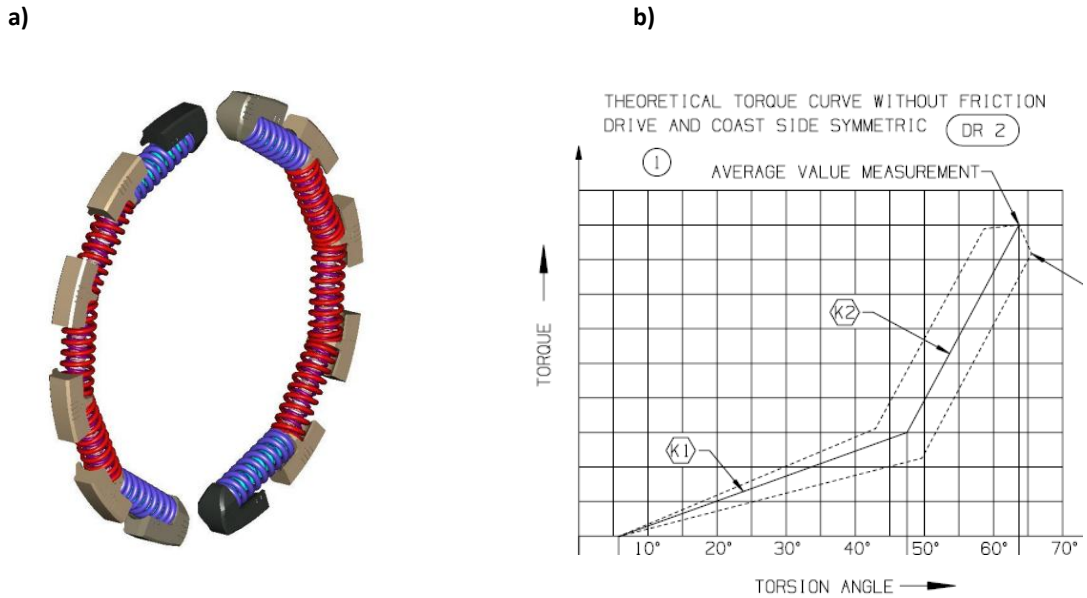

Figura 3.12: a)3D schematic of two-stage spring/damper system; b)Characteristic torque curve of the DMF

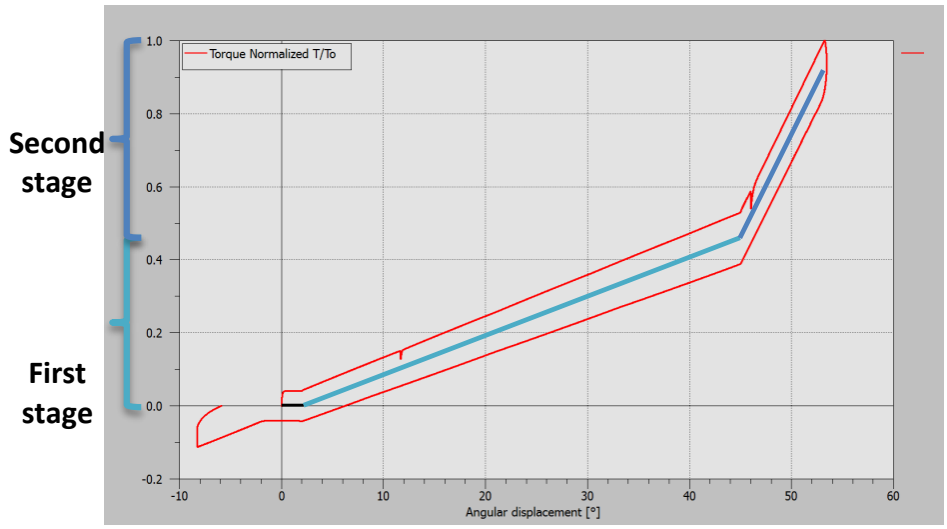

Figura 3.13: Simulated characteristic torque curve of DMF

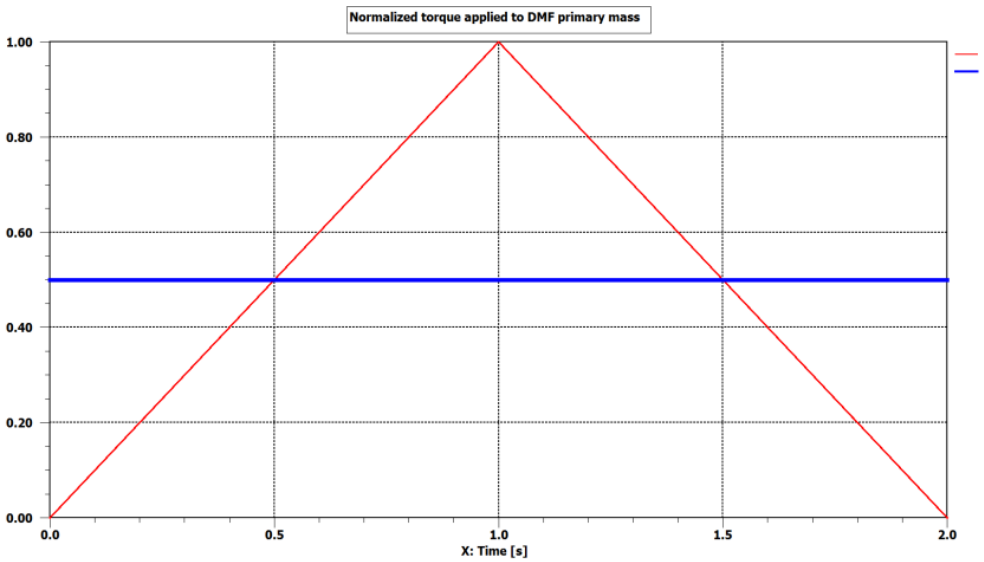

Figura 3.14: Torque applied to DMF with an increasing and decreasing ramp function

In real operating condition, the DMF is uncoupled with the transmission part during engine start and idling. When idling, engine torque is quite small and overcomes only dynamic frictions and inertias. Instead engine start is a critical condition since static friction could be very high at low ambient temperatures (even 70/80 Nm) and also the torque delivered during the first firings, for accelerating the engine inertias, is quite high. However in normal condition the torque will hardly be high enough to bring DMF working in the second stage. Hence considering the DMF operating in the first stage, from the Bode diagram, the magnitude gain can be plotted as a function of engine speed n (rpm) (Figura3.18).

The maximum amplification occurs at an engine velocity around 300 rpm. For such engine velocity the DMF goes into its resonance field and is subjected to a dangerous situation. In normal operating condition, this velocity is reached only at engine cranking. In fact for the actual dual mass flywheels the main disadvantage is their fragility during engine start. In Figura3.19 the velocities of the two sides of the DMF during the engine starting phase are plotted. At around $300 - 400$ rpm the oscillations of the secondary mass becomes remarkable and the system goes out of phase.

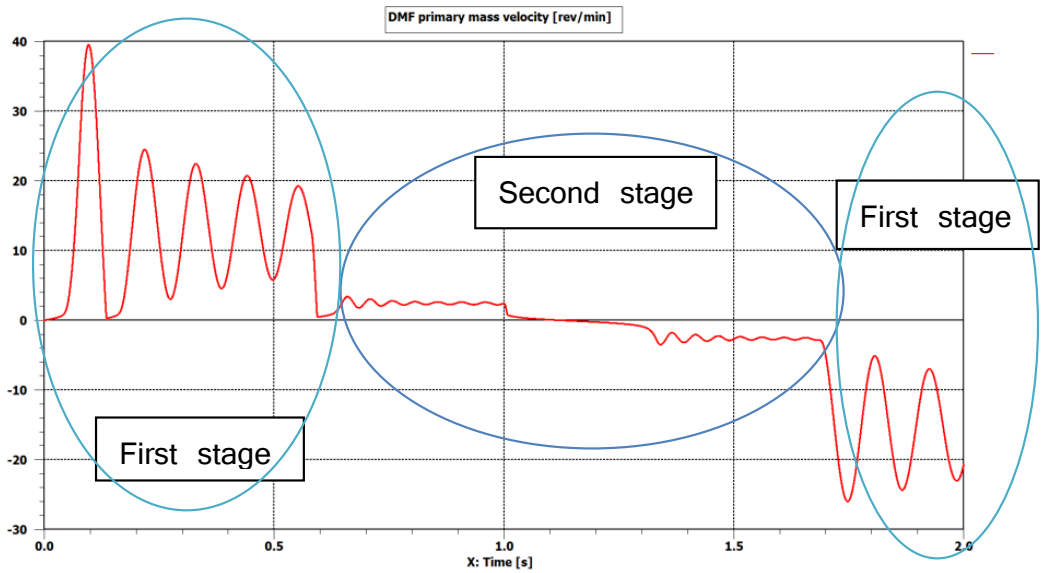

Figura 3.15: Response of DMF to the torque applied: velocity difference of the two masses

3.1.3 Engine

The engine considers a 4-cylinders light-duty passenger car diesel engine. Main engine data and configuration were collected through experimental testing at engine dyno test bench: more in details, in-cylinder pressure waves and friction data were acquired experimentally. Since the aim of this work is to perform a torsional behavior of the starting system, the AMESim model used to simulate the engine is a $2D$ crankshaft-piston model with inertias and frictions effects. It computes the motion of a 4 pistons engine due to the kinematics and the dynamics of the engine rotating masses and calculates the resulting torque on the crankshaft as an effect of inputted in-cylinder pressure. The engine model set up this way cannot be considered as a closed loop system since it requires in-cylinder pressure data to run. These data can be acquired from experimental tests or either derived from thermodynamic equations. This second approach allows to predict pressure values and therefore to arrange a closed loop system, avoiding (or reducing) bench test activities. For this reason a preliminary combustion model for predicting in-cylinder pressure for different engine conditions is set up. In Figure 3.20 the modeling is presented, including the main elements:

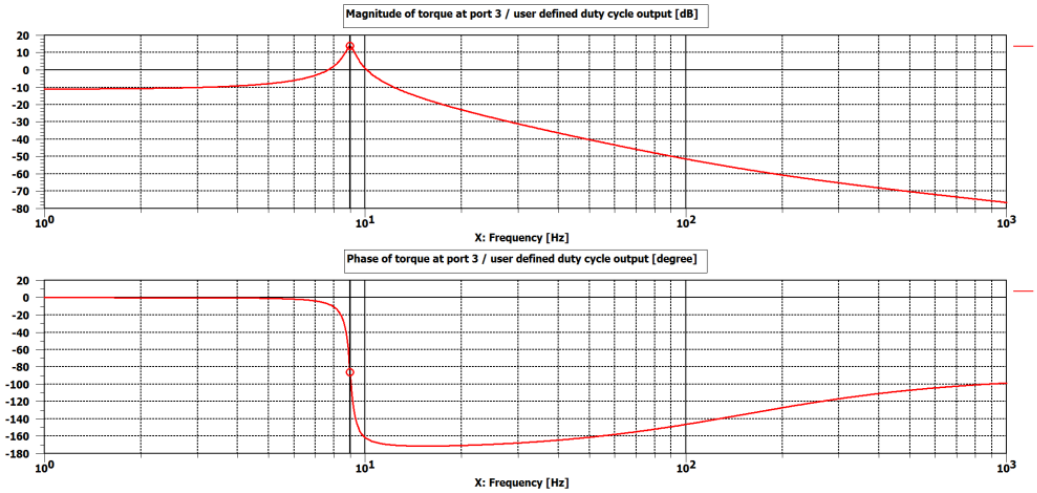

Figura 3.16: Bode diagram of DMF in 1st stage

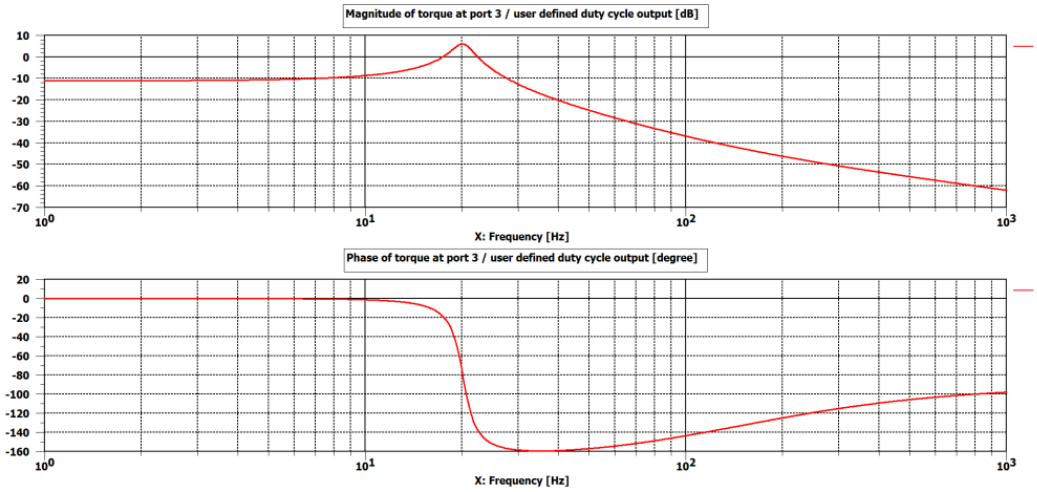

Figura 3.17: Bode diagram of DMF in 2nd stage

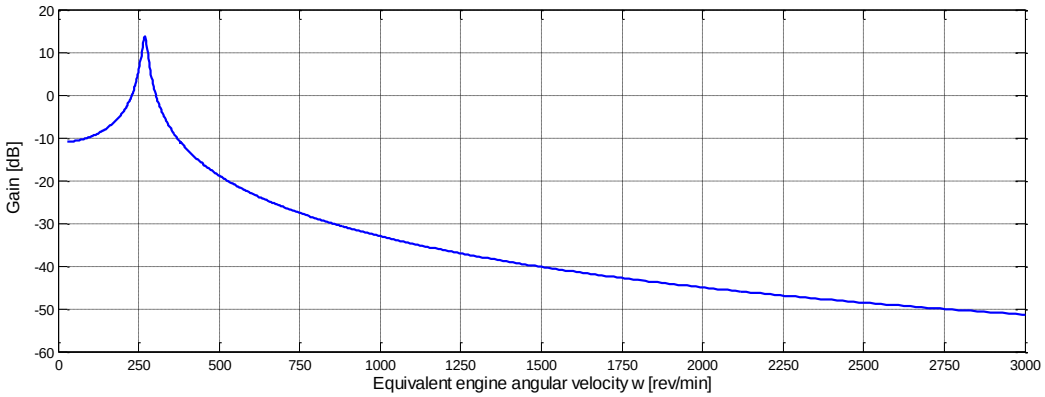

Figura 3.18: Resonance of DMF in 1st stage as a function of engine velocity

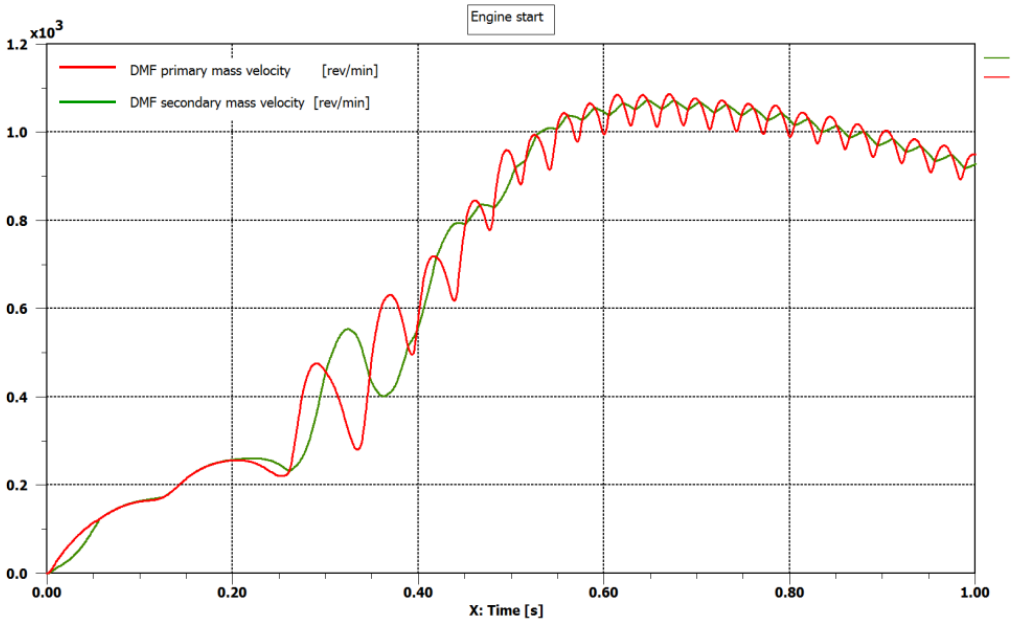

Figura 3.19: Velocities of DMF primary and secondary mass during engine starting phase

- 4 piston/cylinder models for crankshaft dynamic computation;
- Inertia model for rotating and reciprocating masses;
- Friction model;
- In-cylinder pressure data.

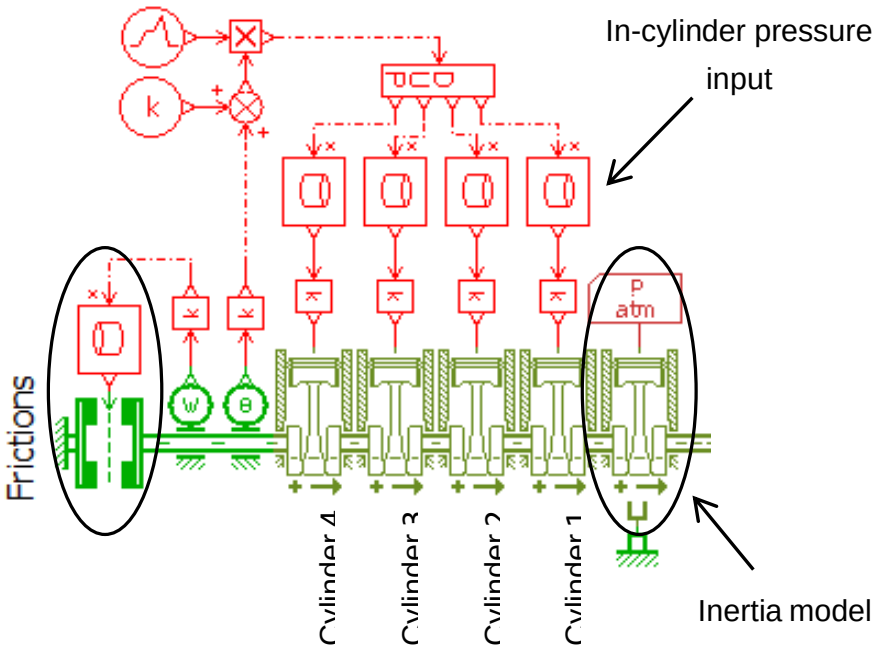

Figura 3.20: Engine modeling in AMESim.

Piston, connecting-rod and crank throw assembly The crankshaft-piston model simulates the effect of the in-cylinder pressure on the crankshaft motion. Considering Figura3.21 schematic, the kinematic and dynamic equations can be computed.

The instantaneous position of the piston is a function of the crankshaft angular displacement given by:

$$x = R \cdot (\cos\theta - 1) - L \cdot \left[1 - \sqrt{1 - (fracR\cot\sin\theta - \Delta L)^2}\right] \tag{3.3}$$

The relative velocity between the piston and cylinder walls is calculated as a function of the rotary velocity of the crankshaft N and the lever arm done by the connecting-rod associated to the crank throw G:

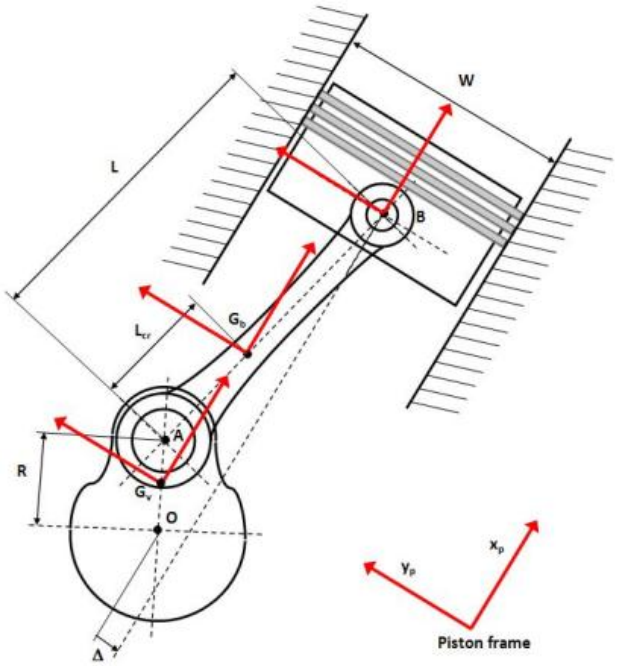

Figura 3.21: Piston, connecting-rod and crank throw assembly schematic.

$$G = R \cdot (\sin\theta - 1) + \frac{R \cdot \sin\theta - \Delta}{\sqrt{1 - (fracR\cot\sin\theta - \Delta L)^2}} \cdot \frac{R}{L} \cdot \cos\theta \tag{3.4}$$

$$V_{relative} = G \cdot N \tag{3.5}$$

The force due to the pressure in the chamber is:

$$F_{P_i} = area \cdot (P_i - P_{atm}) \tag{3.6}$$

The corresponding torque on the crankshaft for each piston is then:

$$T_{P_i} = G \cdot F_{P_i} \tag{3.7}$$

The corresponding torque on the crankshaft for each piston is then:

$$T_{P_i} = G \cdot F_{P_i} \tag{3.8}$$

The model requires therefore the following parameters:

- w, the bore in mm;
- s, the stroke of the piston in mm ($s = 2 \cdot R$);
- L, the length of the connecting-rod in mm;
- Δ, the distance between the translation axis of the gudgeon pin and the crank rotation axis in mm;
- δ, the piston angle (half of the V angle) in degree;
- ϕ, the crank throw angle in degree;
- θ_{c0},the initial angular displacement of the crankshaft in degree ($0^o = TDC$, $180^o = BDC$) In-cylinder pressure is provided as input to the model.

Inertias The inertia model takes into account each inertia of the system to simulate the dynamics of the rotating and reciprocating masses. It includes the inertia of the primary mass of the DMF. The external torque (for example from starter motor) is added to the torque produced by the forces acting on the piston due to in-cylinder pressure. Thus the resulting torque is used to apply the fundamental principle of the dynamic to compute the crankshaft acceleration. The crankshaft velocity is computed by integration of this acceleration. The kinematic constraints generates a Coriolis torque which is the product of the square of the crankshaft velocity (N^2) with an inertia depending of the crank angle $J_i(\theta)$:

$$T_{inertia_i} = J_i(\theta) \cdot N^2 \tag{3.9}$$

The acceleration depends both on the resulting applied torque and on the resulting inertia which is the sum of the crank-piston inertias depending of the crank angle.

$$\frac{dN}{dt} = \frac{1}{\sum J_i} \times T_r \tag{3.10}$$

The crankshaft velocity is the integral of this acceleration.

The following parameters are required:

- moment of inertia of the crankshaft;
- moment of inertia of the primary mass of the DMF;
- moment of inertia, mass and COG (center of gravity) of connecting-rod;
- mass of the piston;
- mass of the crank throws and position of their COG.

In the model it was also added an overall inertia value taking into account all the auxiliary components and accessories directly driven by the engine (camshafts, pulleys, belts, water pump, etc.).

Frictions From the mechanical efficiency definition for an internal combustion engine, the friction work is the portion of the total indicated work, given by the combustion, that is dissipated in a variety of ways within the engine and auxiliaries devices and it is not available at the crankshaft. It can be described therefore by the following aspects:

- Pumping frictions due to losses during intake and exhaust phases;
- Rubbing frictions due to contact between components with relative motion;
- Accessory losses to drive engine essential devices for its operation.

These friction works can be considered as a negative contribution to the system, contrasting engine torque. In general the friction forces are given by elements that are independent of speed (dry friction) and elements that are proportional to speed (dynamic viscous friction). Therefore a speed dependent friction model was considered with in addition a âstictionâ effect at around 0 velocity to simulate static friction that need to be overcome to enable relative motion of stationary objects in contact. This model is shown in Figura3.22

Friction analysis is a complex topic since they depend on several factors, such as component design, working conditions (temperature, in-cylinder pressure, load), lubrication system, leakages, etc. Thus for determining a friction map, several bench test activities were done. Two different approaches were followed: Motoring the engine, with water and oil temperature at standard operating condition (about 90^oC), in order to measure the torque required to overcome engine frictions at different velocities. This measurement represents approximately the sum of pumping, rubbing friction and auxiliary power losses; Measuring in-cylinder pressure while the engine was running at different speeds and loads ($bmep$) allows to determine directly the net indicated power and pumping losses, integrating $\int pdV$. The friction power is therefore given by subtracting the brake power to the indicated power (in terms of mean effective pressure: $fmep = imep - bmep$). While the pumping losses are the area of $P - V$ (Pressure vs. Volume) diagram during intake and exhaust stroke. The friction torques measured with the first method includes generally all kind of losses and therefore it is useful when the in-cylinder pressures, provided as input in the piston model, are calculated from thermodynamic equations in which for example pumping losses are not considered (intake and

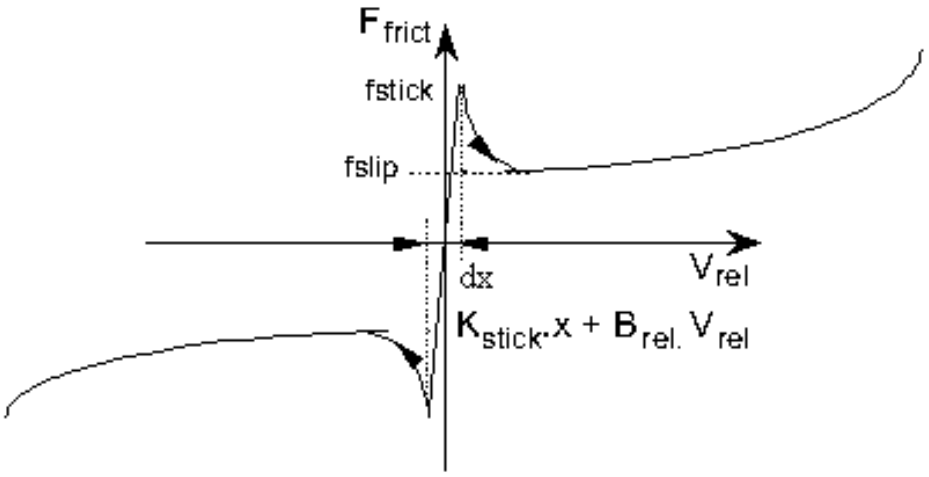

Figura 3.22: Friction model as a function of relative speed with stiction effect.

exhaust stage are ideally performed at constant ambient pressure). Therefore, as it will be described in the following chapter, the friction values acquired from this approach were used when the pressure data were predicted by simulation through a combustion model. Whereas measuring in-cylinder pressure allows to determine separately the pumping frictions, through $\int pdV$ over the intake and exhaust stages, and the sum of rubbing frictions and auxiliaries power, through $\int pdV$ over the combustion cycle, minus load (brake torque) applied. When experimental data of in-cylinder pressure are used for running the engine model simulation, the pumping losses are already considered in the resulting torque computation.

Hence only the effects of rubbing frictions and auxiliaries power losses are added to the system as a contrasting effect to engine torque. In order to validate the engine model it was necessary to manually slightly modify the friction values in order to achieve fitting between simulation and experimental results. Moreover it was not possible to have friction measurements at engine speed lower than 700 rpm. In fact the engine shows deep vibrational problems at low speed regimes and it is therefore avoided to run in these conditions. Moreover the measuring instruments are not designed to perform at low velocities. Some assumptions were made in order to complete missing data and the final result is plotted in the Figura3.23.

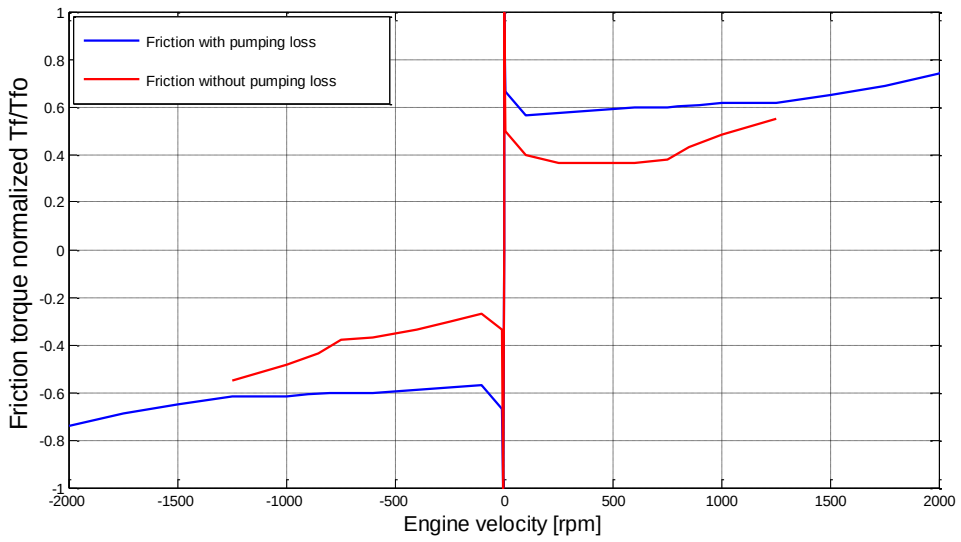

Figura 3.23: Friction map from the two methods: motoring and considering pumping losses; work integral over the combustion cycle not considering pumping losses.

The plot shows the curves of friction torque vs. engine speed resulting from the two methods (motoring: the sum of pumping, auxiliaries and rubbing frictions; work integral over the combustion cycle: the sum of only auxiliaries and rubbing frictions). The friction model control system is consequently based on detecting the instantaneous engine velocity, interpolating the friction curve and returning the resulting torque to the system.

In-cylinder pressure In-cylinder pressure data is an input to the piston-crankshaft model, which provides to calculate the resulting engine torque. As a starting point, in order to validate the model, pressure inside the 4 cylinders was measured in bench test activities during motoring and engine start phase. It is however clear that having a closed loop system, which can simulate and predict in-cylinder pressure waves for different engine conditions, can bring to remarkable time and cost benefits. Glow plug pressure sensors are used for in-cylinder acquisitions. Two conditions were considered for validating the whole starting system:

1. Motoring the engine through the starter motor without any combustion (without fuel injection);
2. Starting the engine till it reaches the idle state. For both conditions absolute pressure data were collected as a function of crankshaft angle position for the four cylinders. The pressure waves were analyzed and rearranged. They are shifted of 180^o for each cylinder. The firing order is $1-3-4-2$.

They are presented as a function of the crankshaft angle respectively in in Figura3.24 and Figura3.25.

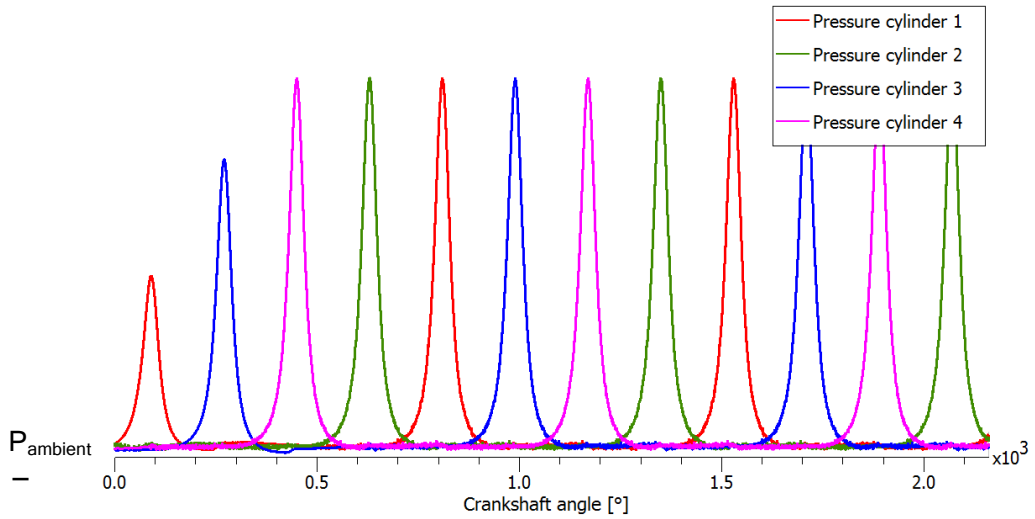

Figura 3.24: In-cylinder pressure during engine motoring vs. crankshaft angle.

The control system for the in-cylinder pressure consists in reading the instantaneous angular position of the crankshaft and transmitting the correspondent pressure value to the piston system.

3.1.4 Model validation

Simulations of the whole starting system model, as described, were run. The results were compared to experimental data in order to validate the model. In particular during test activities the engine velocity was monitored and associated to the correspondent in-cylinder pressure data collected. This velocity

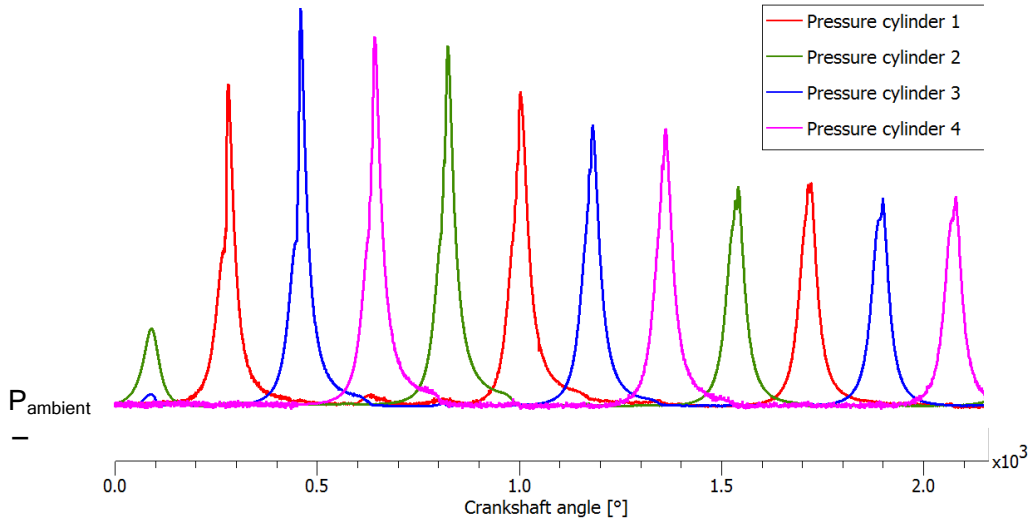

Figura 3.25: In-cylinder pressure during engine starting phase vs. crankshaft angle.

was compared to the simulated crankshaft velocity Figura3.26. Considering the case of cranking the engine through starter motor, contact stiffness between teeth and backlash can be taken into account. These effects are plotted in Figura3.27.

For engine starting simulation, the experimental data consists of the mean velocity of the engine crankshaft in time. The results are compared to this available data Figura3.28.

From the result analysis it comes out that the model simulates good enough the engine start phase. The correspondence with the experimental data validates hence the modeling and components parameterization. The main limit of the model is its open loop nature. That is the simulations are linked to specific cases with dedicated data collection (as for in-cylinder pressure). Therefore it cannot guarantee accurate results for different cases and conditions without relative data. A closed loop system can be completed if the in-cylinder pressure values are also simulated by the model. The pressure inside the cylinder during motoring and combustion can be predicted from thermodynamics equations and a preliminary study for this purpose is presented.

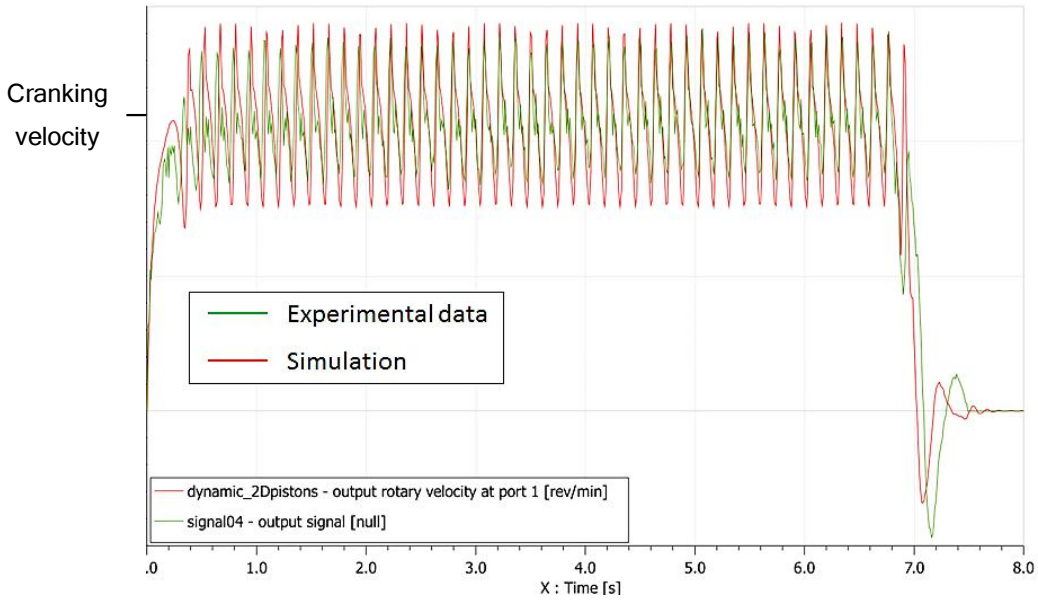

Figura 3.26: Engine cranking velocity with ideal gear meshing.

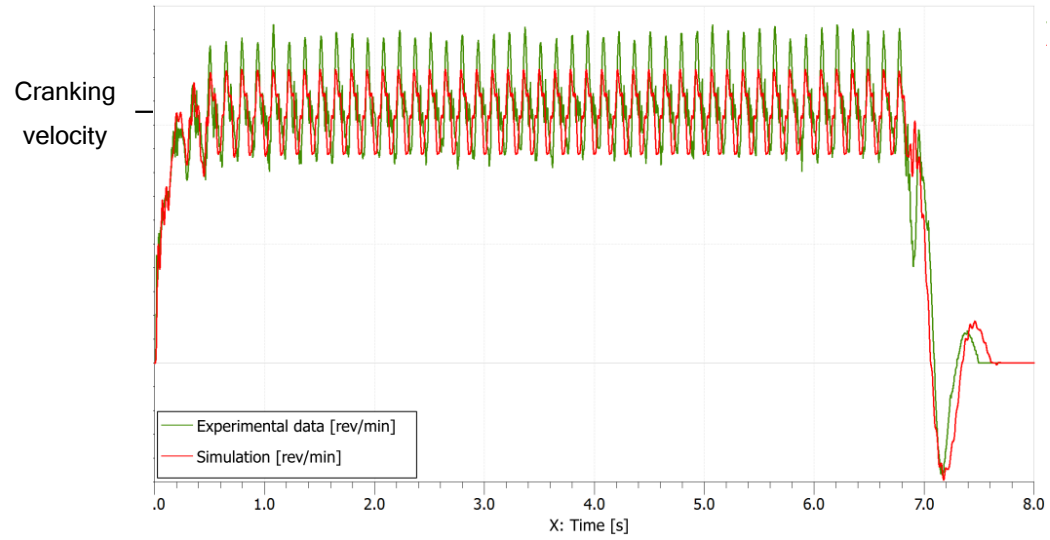

Figura 3.27: Engine cranking velocity with stiffness and backlash between gears.

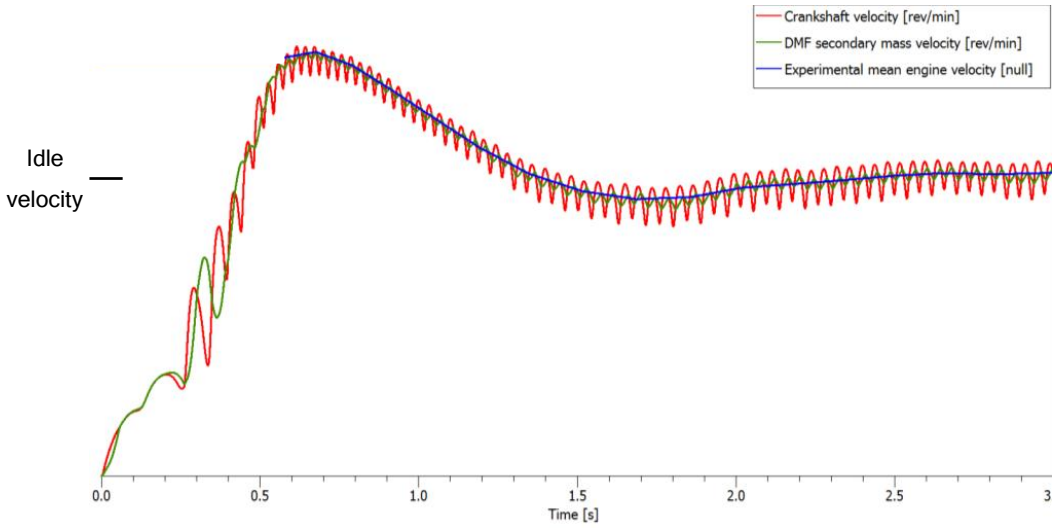

Figura 3.28: Simulation of engine velocity during starting.

3.2 Transmission

The engine delivers useful power to the vehicle through the transmission components. The transmission adapts the output torque of the engine to the drive wheels. The main components are:

- Clutch;
- Gear box:
  - Primary shaft (input shaft)
  - Gears
  - Secondary shaft (output shaft)
- Differential (with final drive ratio)
- Axel shafts (half-shafts)
- Wheels:
  - Tires.

When the clutch is engaged, the engine is directly coupled with the transmission and can deliver torque to the gearbox input shaft, which is rigidly connected to the clutch disk. The gearbox has the function to generate a desired transmission ratio through two meshing gears. The second gear is driving the output shaft. A set of gear ratios could be obtained selecting different gears inside the gearbox. The output shaft torque is in turn delivered to the differential through a bevel gear with a final drive ratio. Finally from the differential the torque is delivered through the axel shafts to the wheels that provide traction to the vehicle by tire contact with the road.

A schematic overview of the powertrain is shown in Figura3.29.

A simplified schematic model of the complete powertrain is shown in Figura3.30.

Considering the transmission ratios, the angular velocity of the powertrain parts can be related to the wheels velocity as:

$$\begin{aligned} &V_{veh} = \omega_w \cdot R_w \quad \text{where } R_w \text{ is the wheel dynamic radius} \\ &\omega_{diff} = \omega_w \\ &\omega_{gout} = \omega_w \cdot i_{FD} \\ &\omega_{eng} = \omega_{DMF} = \omega_{clutch} = \omega_{gin} = \omega_w \cdot i_{FD} \cdot i_g \end{aligned} \tag{3.11}$$

In steady state conditions, the power transmitted from the engine available to the wheels is affected by losses through the transmission. Therefore an efficiency coefficient ($\eta_{tr} < 1$) can be introduced:

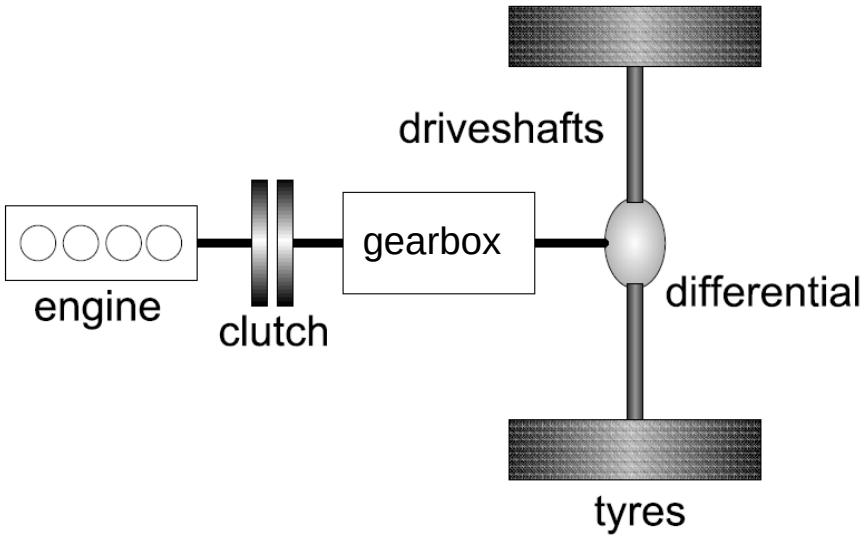

Figura 3.29: Schematic overview of powertrain.

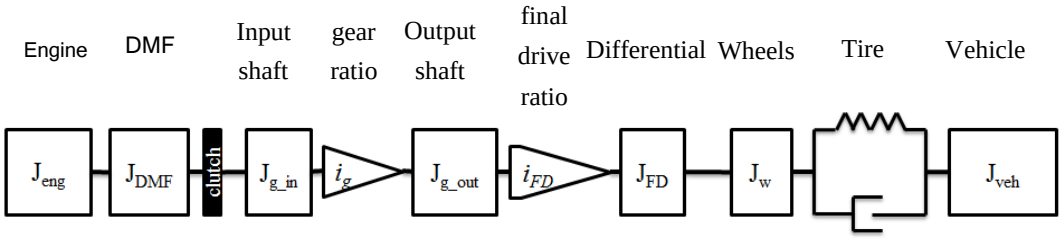

Figura 3.30: Powertrain simplified model.

$$P_w = \eta_{tr} \cdot P_{eng}$$

Since the power can be expressed as

$$\mathrm{P}_{eng} = T_{eng} \cdot \omega_{eng}$$

The torque delivered from the engine available to the wheels is accordingly:

$\mathrm{T}_w = \eta_{tr} \cdot T_{eng} \cdot i_{FD} \cdot i_g$
(3.12)

In Figura3.31 a the engine velocity is compared to the resulting wheels velocity when the vehicle is traveling at 50 km/h in 4th gear. While the Figura3.31 b shows a comparison between the engine torque and the one delivered to the vehicle.

The transmission modeling in AMESim is shown in Figura3.32.

3.2.1 Clutch

The clutch is necessary to connect the flywheel to the gearbox shaft. Its purpose is to transmit power with little slippage. This is basically done using a friction disk that is brought gradually in contact with the two sides through a spring (or actuator) in order to match their different rotating speed progressively. The clutch system is shown in Figura3.33. The clutch disc is mounted onto the transmission input shaft and is radially fixed by a splined interface. The clutch is normally closed, as the diaphragm spring is pre-tensioned when assembled. The axial bearing can slide over the transmission input shaft and push against the fingers of the diaphragm spring. The direction of the release force is swapped through the lever joints and releases the pressure from the clutch disc, which is then able to rotate independently from the engine.

On the engine side, the pressure plate is rigidly attached to the flywheel. For the transmission considered in this project, it is bolted to the secondary mass of the DMF. The conventional clutches are equipped with torsional spring/damper system to reduce chatter. But when a DMF is mounted, the

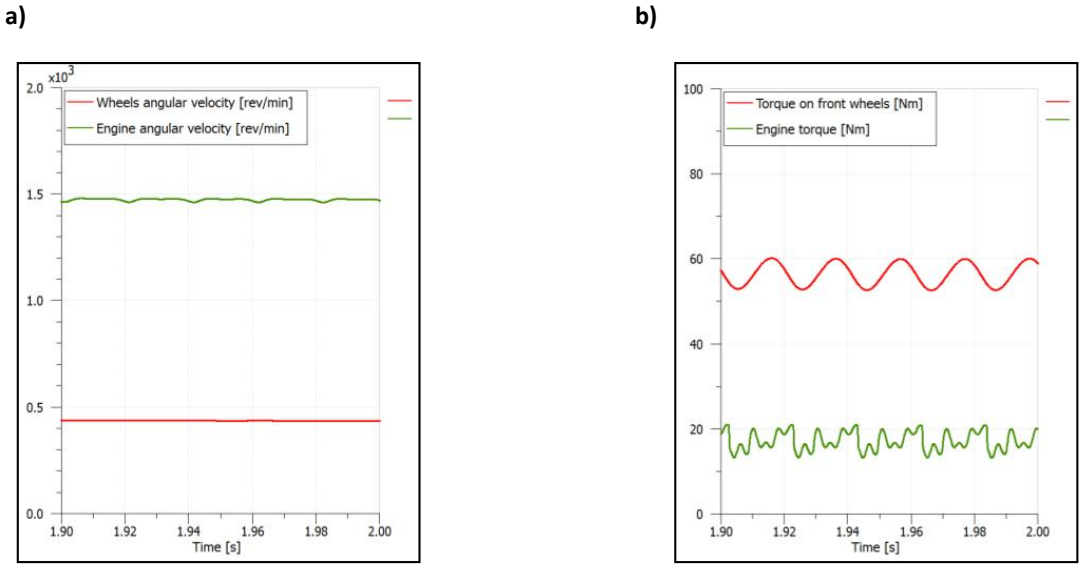

Figura 3.31: (a) Wheels velocity and engine velocity at 50 km/h in 4^{th} gear. (b) Torque on wheels and engine torque in 4^{th} gear.

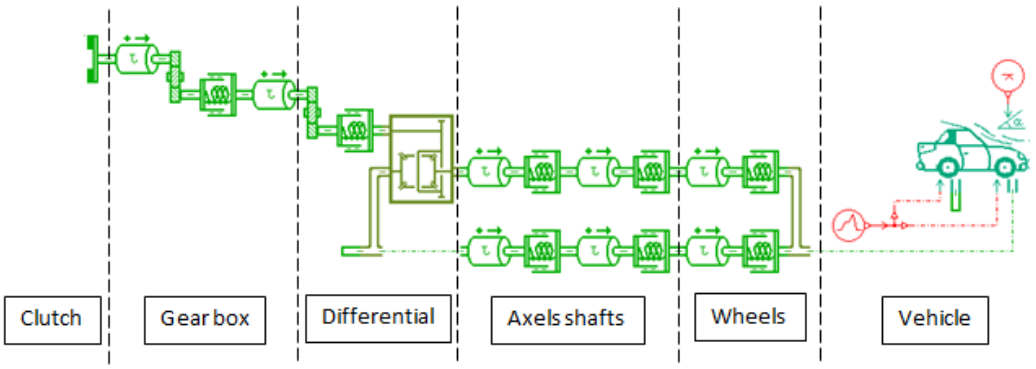

Figura 3.32: Transmission modeling in AMESim.

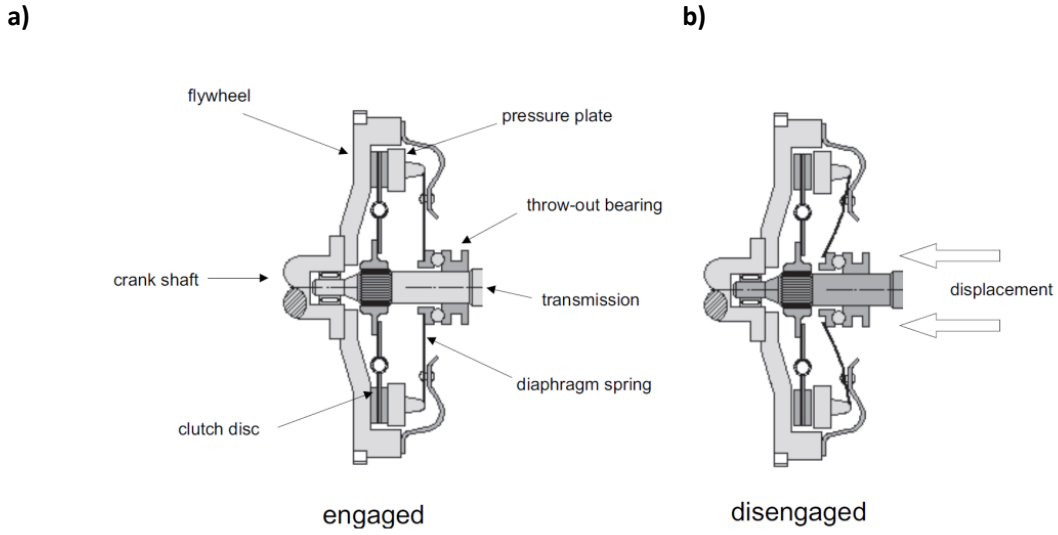

Figura 3.33: Clutch system schematic.

vibrations and engine irregularities are damped by the elastic elements of the DMF itself. This allows the use of a simpler clutch that works only by contact friction. There are essentially three distinct modes of operation of the clutch:

- Free state, where the clutch is completely disengaged and transmits no torque through the two sides, which are independent of each other.
- Lockup state, where the clutch is fully engaged and the engine is rigidly coupled to the driveline. Therefore the two sides of the clutch have the same velocity.
- Slipping state is the intermediate condition, in which the two sides have different angular velocities and the clutch is acting a gradual friction force to match them and bring to the lockup state.

The torque transmitted through the clutch is denoted by T_c. In the free state condition it is evidently 0. While in lockup state, or sticking condition, it is the total engine torque that is transmitted through the clutch. The sticking of the clutch sustains as long as the torque transmitted through the clutch remains below the maximum transmissible torque T_{cmax}.

This torque is given by:

$$\begin{aligned} T_{cmax} &= F_{nmax} \cdot \mu_0 \cdot R_a \\ T_c &\leq T_{cmax} \end{aligned} \tag{3.13}$$

Where F_{nmax} is the maximum actuation force working on the clutch plate, μ_0 the static friction coefficient of the clutch surface material and R_a the effective radius of the clutch plate. In slipping state the two sides are rotating with different velocities and the system is subject to dynamic variations. Assuming a Coulomb friction model, the torque through the clutch during slipping is given by:

$$T_c = F_n \cdot \mu \cdot R_a \cdot (\omega_{eng} - \omega_{clutch}) \tag{3.14}$$

Where F_n is the actuation force working on the clutch plate (exerted by the diaphragm spring or by an hydraulic or pneumatic actuator system), μ the dynamic friction coefficient of the clutch and R_a the effective radius of the clutch plate. ω_{eng} and ω_t are respectively the engine angular velocity and the transmission input shaft velocity. The sign of their difference suggests the direction of the torque. For example, when the transmission velocity is greater than the engine velocity, the vehicle inertia is driving the engine. Since the transmitted torque is proportional to the axial actuation force F_n, the control can be managed acting on the actuation system.

From the simulation point of view, the Coulomb model is a static model and it is inadequate to describe dynamic systems. The Coulomb friction model equation, as already described, can be simplified as:

$$T_c = T_{dyn} \cdot (\Delta\omega) \tag{3.15}$$

where T_{dyn} is the dynamic friction torque. The Coulomb friction model is illustrated in Figura3.34a. Because the equation of motion for dynamic systems is strongly non-linear with a Coulomb friction model, a tanh function can be employed to ensure the transition through zero and limit the friction torque. The hyperbolic tangent model equation is given by:

$$T_c = T_{dyn} \cdot \tanh\left[k \cdot \frac{\Delta\omega}{\Delta\omega_0}\right]) \tag{3.16}$$

where k and $\Delta\omega_0$ are coefficients that determines how fast the tanh function changes. Tanh model is illustrated in 3.34b and compared to the Coulomb model.

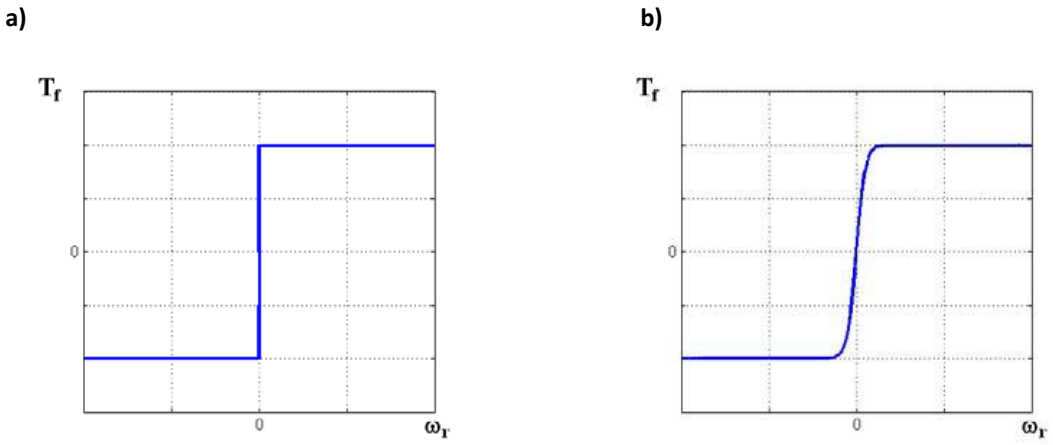

Figura 3.34: (a) Coulomb friction model. (b)Tanh friction model.

Another dynamic model that can be used is the Dahl model. Dahl model is a generalization of the ordinary Coulomb equation, that is, the steady-state version of Dahl model is the Coulomb friction. Dahlâs differential expression for friction is inspired from elasto-plastic behavior of materials. It is formulated as:

$$\frac{dT_c}{dt} = K \cdot \Delta\omega \cdot \left[1 - \frac{Tc}{T_{dyn}}(\Delta\omega)\right]^{\cdot} \left[1 - \frac{Tc}{T_{dyn}}(\Delta\omega)\right] \tag{3.17}$$

Where K is the torsional stiffness coefficient and is a parameter that determines the shape of the stress-strain curve. In the literature, the Dahl model is often simplified with the exponent $= 1$. Then:

$$T_c = F_n \cdot \mu \cdot R_a \cdot (\omega_{eng} - \omega_{clutch}) \tag{3.18}$$

The torque transmitted through the clutch can be derived from numerical integration.

For the purpose of this project some simplifications are made:

- the thermal effects are not taken into account because they have a low dynamic and influence most of all the friction coefficient μ, which is considered constant.
- the friction torque is computed using a normalized $0-1$ command signal (com) as a fraction of the maximum friction torque, that is:

$$T_{dyn} = com \cdot T_{cmax}) \tag{3.19}$$

Furthermore as a starting point a tanh model was sufficient to achieve proper results. The AMESim clutch model, used in a manual gearbox, is shown in Figura3.35.

Figura 3.35: Clutch system schematic.

The command of the clutch is 1 (100%) when disengaged and 0% when released (engaged). The control of the clutch will be discussed in chapter 4.

3.2.2 Gearbox, differential and final drive

The gearbox input shaft is connected to the friction plate of the clutch. The output shaft is driven by the input shaft through a gear mesh and is connected to the differential via the final drive. The bevel gear drives the differential with another transmission ratio which is fixed. The drive shafts connect the satellites of the differential to the wheels. Since only straight line driving is considered, they are assumed to have the same velocity. The effects on torque and speed in the gearbox and final drive include:

- Torque multiplication and speed reduction via the gear ratios;
- Torque losses due to the acceleration of rotational inertias;
- Torque losses due to the friction between meshing gears.

The gear ratios of the gearbox and of the final drive are defined as:

$$\begin{aligned} i_g &= \frac{\omega_{gin}}{\omega_{gout}} \\ i_{FD} &= \frac{\omega_{gout}}{\omega_{gw}} \\ i_{tot} &= i_{FD} \cdot i_g \end{aligned} \tag{3.20}$$

Since the gearbox input shaft is connected to the clutch, the torque delivered to the final drive (differential, axel shaft and wheels) can be expressed as:

$$\begin{aligned} T_w &= \eta_{tr} \cdot T_c \cdot i_{fd} \cdot i_g - J_{gin} \cdot i_g \cdot i_{FD} \cdot \omega_{gin} - J_{gout} \cdot i_{FD} \cdot \omega_{gout} - J_{Diff} \cdot \dot{\omega}_w \\ &= \eta_{tr} \cdot T_c \cdot i_{fd} \cdot i_g - \left(J_{gin} \cdot i_g^2 \cdot i_{FD}^2 + J_{gout} \cdot i_{FD}^2 + J_{Diff}\right) \cdot \dot{\omega}_w \\ &= \eta_{tr} \cdot T_c \cdot i_{fd} \cdot i_g - J_d \cdot \dot{\omega}_w \end{aligned} \tag{3.21}$$

where $J_d(i_{FD}, i_g)$ is the lumped inertia of all rotating transmission and driveline parts, which is a function of transmission ratios.

$$J_d = J_{gin} \cdot i_g^2 \cdot i_{FD}^2 + J_{gout} \cdot i_{FD}^2 + J_{Diff} \tag{3.22}$$

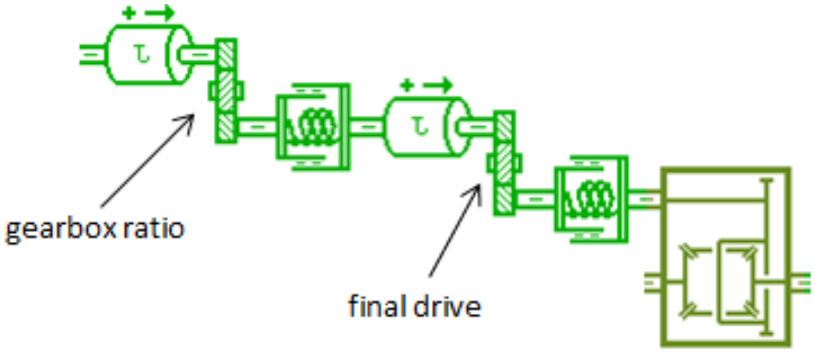

Figura 3.36: Transmission modeling in AMESim.

3.2.3 Wheels and vehicle

The drive torque T_w is the torque at the wheels. Via tire-road interaction, this results in longitudinal acceleration of the vehicle. The model structure assumes the driving wheels and tires as inertial components connected to the vehicle through a linear stiffness and damping. In general the governing equation of motion is given by:

$$J_w \cdot \dot{\omega}_w = T_w - R_w \cdot F_x \tag{3.23}$$

with J_w the wheels inertia, $\dot{\omega}_w$ wheels angular acceleration, R_w the dynamic wheel radius and F_x the tire friction force. This force is defined as:

$$F_x = F_2 \cdot \mu(\kappa, , F_z) \tag{3.24}$$

where the tire friction coefficient $\mu(\kappa, , F_z)$ is a non-linear function dependent on the longitudinal slip κ, side slip angle and tire vertical load F_z. The most common tire friction model used in the literature is the so-called *Magic Formula* or *Pacejka model*, which uses static maps to describe the relation between slip and friction. Though, a detailed behavior analysis of the tire is not required to study clutch behavior. Therefore an ideal non slipping condition is considered.

The vehicle acceleration depends on the torque delivered from the tires. A travelling vehicle is subjected to different resistive loads, such as air resistance, rolling resistance, road inclination. Therefore the equation of dynamic equilibrium can be written as:

$$m_v \cdot \dot{v}_v = F_x - F_{res} \tag{3.25}$$

with m_v the vehicle mass, $\dot{v}_v$ the vehicle acceleration, F_x the tire friction force and F_{res} the resistive force. F_{res} can be determined through a coast-down test[3]. It defines the typical vehicle characteristics:

- Aerodynamic drag;
- Tire rolling resistance;
- Wheel bearing and brake drag;
- Axle and transmission spin loss.

These two last elements defines essentially the transmission efficiency coefficient (η_{tr}), which is therefore already counted in the experimental F_{res}. F_{res} is defined by three *coast-down* parameters (coastdown parameters) a [N], independent on vehicle speed, b [N/(km/h)], proportional to vehicle speed and c $[N/(km/h)^2]$, proportional to speed squared. Considering also a road inclination, the formulation of F_{res} is:

$$F_{res} = a + b \cdot v_v + c \cdot v_v^2 + m_v \cdot g \cdot \sin\theta \tag{3.26}$$

[3]Coast-down test consists in launching the vehicle at a certain speed, disengage engine from drive-line and instantaneously recording its speed and traveled distance until vehicle stops. Then speed values over time are interpolated via a second-grade polynomial function.

with v_v the vehicle velocity, m_v the vehicle mass, g the acceleration due to gravity and θ road inclination. The coast-down parameters define the resistive load. Vehicle coasting speed as a result of the simulation (0 road inclination) is shown in Figura3.37.

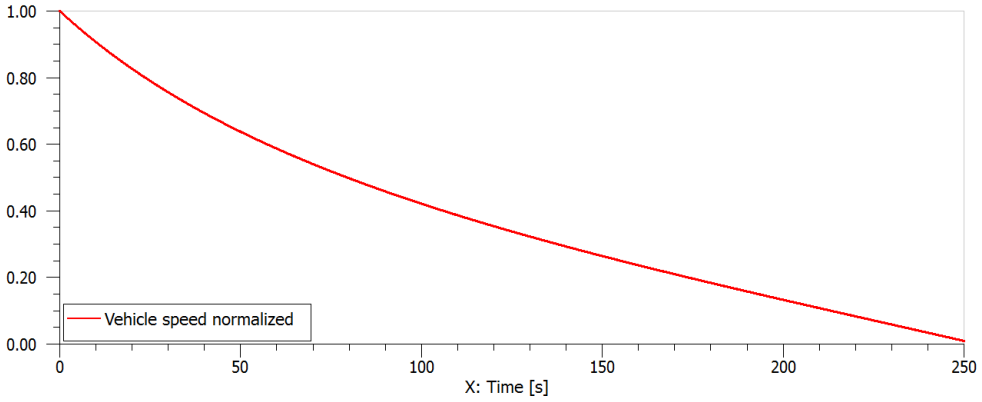

Figura 3.37: Vehicle velocity trend for a coast-down test simulation with 0 road inclination.

From the previous equations, the relation between torque transmitted from tires and vehicle acceleration can be found:

$$\begin{cases} J_w \cdot \dot{\omega}_w = T_w - R_w \cdot F_x \\ m_v \cdot \dot{v}_v = F_x - F_{res} \end{cases} \\ m_v \cdot \dot{v}_v = \frac{T_w}{R_w} \cdot \dot{\omega}_w - F_{res} \tag{3.27}$$

Since $\dot{v}_v = R_w \cdot \dot{\omega}_w$ the equation can be written as:

$$\left(m_v + \frac{J_w}{R_w^2} \right) \cdot \dot{v}_v = \frac{T_w}{R_w} - F_{res} \tag{3.28}$$

This means that the vehicle mass and the wheels inertia can be consider as a lumped vehicle mass m_{vw} (slipping of the tires is neglected), expressed as:

$$m_{vw} = \left(m_v + \frac{J_w}{R_w^2} \right)$$

Resulting in $m_{vw} \cdot \dot{v}_v = \frac{T_w}{R_w} - F_{res}$

(3.29)

3.2.4 Validating modeling of transmission components

The transmission components, from clutch to wheels, do not have infinite stiffness and therefore are subjected to vibrational modes. As showed in **??**, the first step to validate the model of the drive-line is to analyze vibration modes. The modeling of the transmission describes them by their inertia and stiffness (Figura3.38). The main damping effect is achieved from the tires.

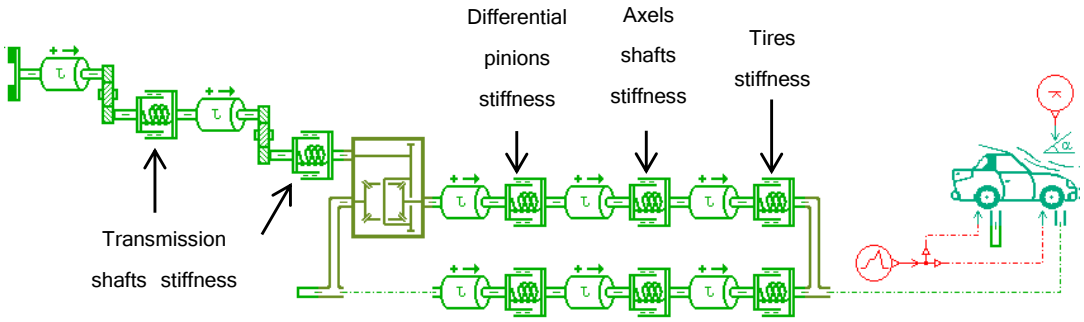

Figura 3.38: Transmission modeling in AMESim with indicated torsional stiffnesses.

For such task wheels are considered as a simple torsional load without slip with respect to the ground and the torsional stiffness of the tire is supposed to be constant. Gears contact stiffness is also considered to be ideal since it does not influence significantly the main vibrational modes. Considering the equivalent simplified model for the transmission system, the dynamic equilibrium equation is defined by J_d ($i_F D$,i_g). It is the lumped inertia of all rotating transmission and driveline parts, and is a function of transmission ratios.

$$J_d = J_{gin} \cdot i_g^2 \cdot i_{FD}^2 + J_{gout} \cdot i_{FD}^2 + J_{Diff} + J_w \tag{3.30}$$

From the definition of J_d, the inertia of the overall system depends on the final drive ratio i_{FD} and on the gear ratio i_g. The final drive ratio is constant but the gear ratio is selected by the driver. Therefore for different gear selections the lumped inertia of the system changes. Since the frequency of vibration depends on the inertia of the system, it will result in different vibrational modes for different gear ratio selected. Therefore the frequency analysis for the drive-line is extended to each

of the six gear ratios for the gearbox considered. In order to visualize the vibration of the drive-line model, a step torque is applied to the clutch. The response of the system is shown plotting the output torque on the wheels and the Bode diagram for each gear ratio.

The results of the frequency analysis for the driveline can be directly read in the plots. The vibrations induced in by the step torque are displayed and the response of the system in frequency domain is present in the Bode diagrams. Since in the case considered the engine is not coupled with the driveline, the irregularities of its motion doesnât affect the system.

3.3 Analysis of vibrations of the drive-line

Frequency analysis is the major point in the evaluation of the impact of powertrain components on drivability. Every system modeled by means of inertial components with stiffness properties, is subjected to oscillatory modes. In the case of power transmission systems using rotating shafts and couplings it is a matter of torsional vibration, that is an angular vibration of a shaft along its axes of rotation. The actual engine crankshaft rotation is characterized by an oscillatory motion caused by compression and expansion strokes of each cylinder and by inertia of rotating and reciprocating masses. Because no material can be infinitely stiff, these alternating torques applied at some distance on a shaft cause twisting vibration about the axis of rotation. These vibrations can cause attached components to fail when the frequency of vibration matches the torsional resonant frequency. Considering a translational spring-mass oscillators system, the general equation of motion is the following differential equation:

$$I\frac{d^2\theta}{dt} + C\frac{d\theta}{dt} + k = T(t) \tag{3.31}$$

Where θ is the angle of deflection, I moment of inertia, C rotational damping, k torsional stiffness. In general the frequency of vibration is very near to the natural resonant frequency of the system, that is:

$$f_n = \frac{\omega_n}{2\pi} = \frac{1}{2\pi}\sqrt{\frac{k}{I}} \tag{3.32}$$

In general mechanical resonance is the tendency of a mechanical system to respond at greater amplitude when the frequency of its oscillations matches the system's natural frequency of vibration (its resonant frequency) than it does at other frequencies. Regarding vehicle powertrain, the designing must ensure that mechanical resonant frequencies of the components do not match driving vibrational frequencies of the resulting engine oscillating motion. For an internal combustion engine,

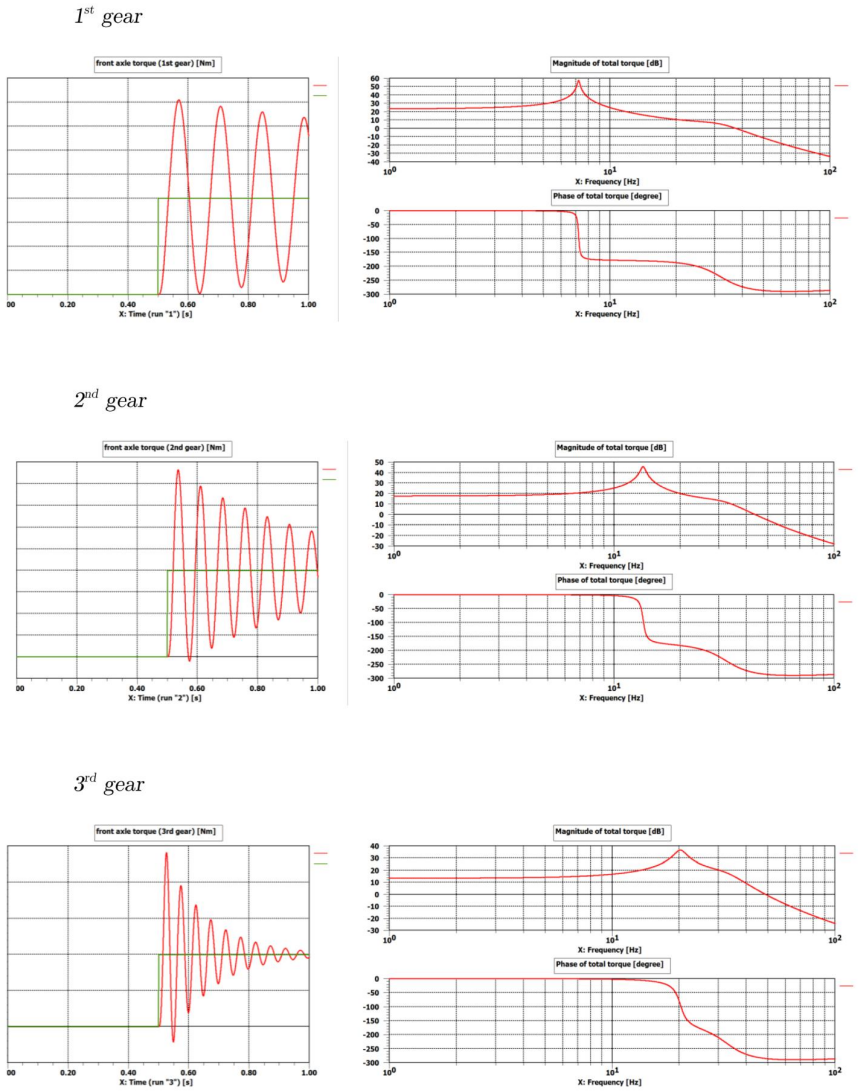

Figura 3.39: Vibrational modes of the transmission for gear 1^{st} to 3^{rd}.

vibration caused by the inertia of the alternating masses is less relevant at low engine velocity with respect to the oscillation caused by gas pressure variation. Since the project is focused on engine start phase, low velocities are considered and the main

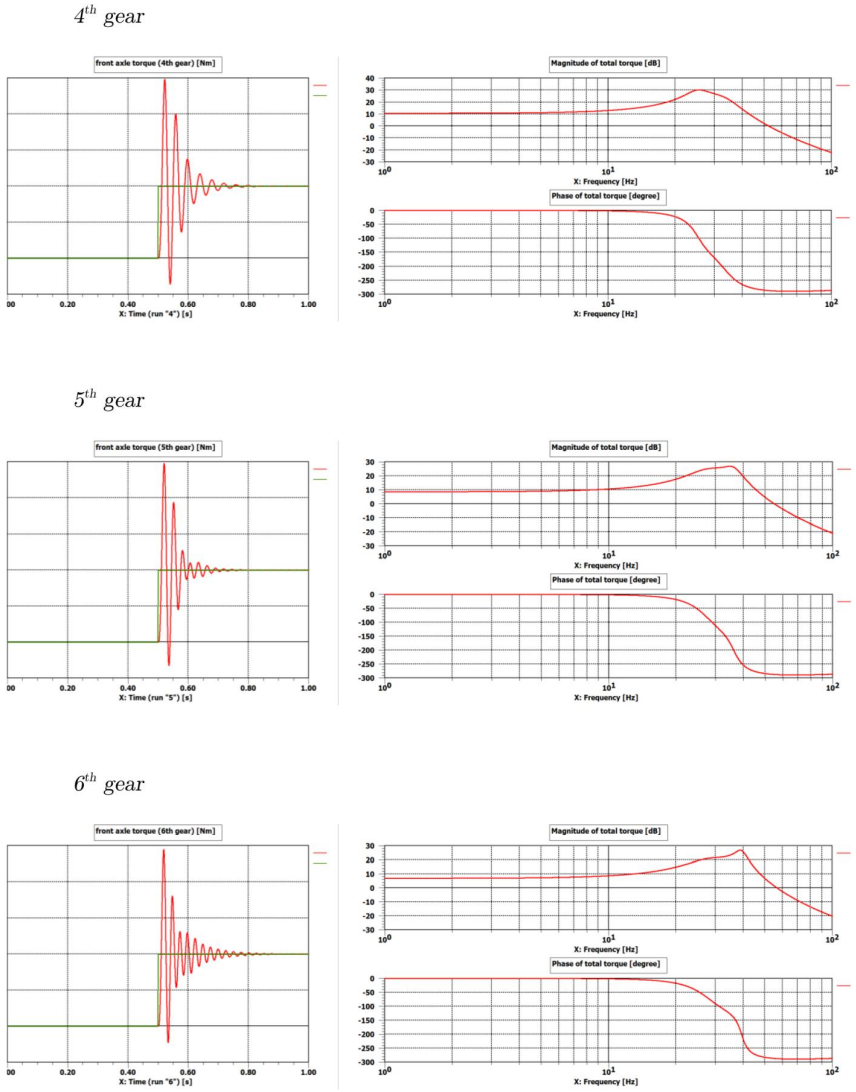

Figura 3.40: Vibrational modes of the transmission for gear 4^{th} to 6^{th}.

contribution for vibration is due to in-cylinder gas pressure during compression and expansion stroke.

For a 4 cylinders 4 stroke engine, at each revolution of the crankshaft (every

360°), there are 2 compression/expansion stages accomplished by 2 consecutive pistons in their firing order. Approximating the oscillatory motion as sinusoidal, the main frequency involved can be calculated considering the engine speed as follows:

$$f_n = \frac{n}{60} \cdot 2 \tag{3.33}$$

where n is the engine speed in revolution per minute.

Actually the oscillatory motion of the crankshaft can be described by a Fourier series, considering the sum of a set of simple oscillating functions. Applying a fast Fourier transform (FFT) to the engine velocity in time it is easy to show the main frequencies composing it. In Figura3.41 it is presented the oscillating velocity of the crankshaft (and secondary mass of the DMF) and the resulting fast Fourier transform diagram.

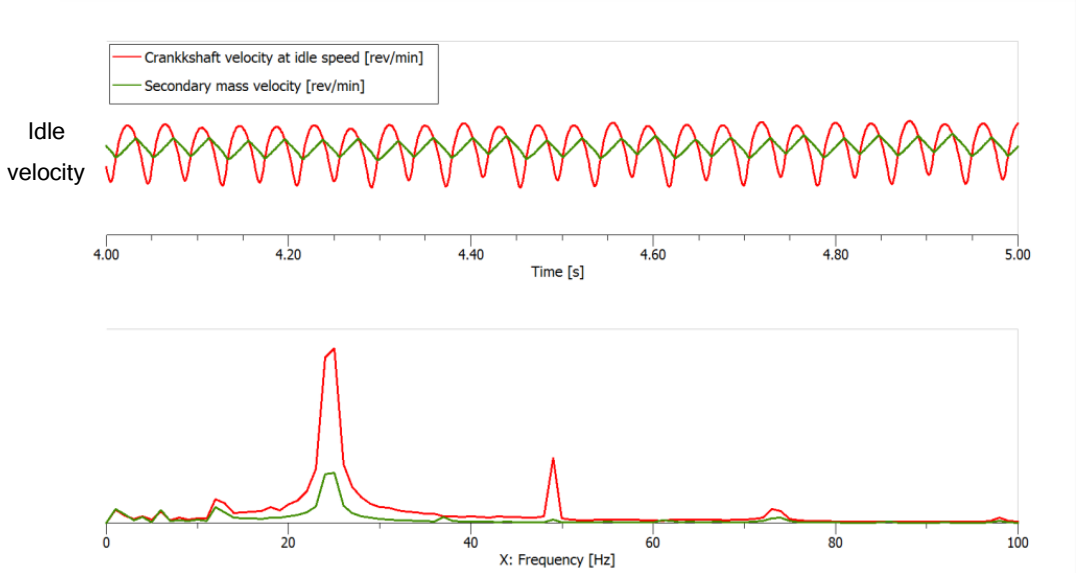

Figura 3.41: Fast Fourier transform of engine velocity at idle.

From the FFT curve it is clear that the frequency of highest amplitude is located exactly at idle speed. Therefore as the frequencies of the engine at speed range of operation are known, the vibrational frequencies of the driveline components are designed not to match those of the crankshaft motion.

Friction has a damping effect, slowing the motion of the system. Damping reduces the amplitude of oscillations and it is linearly related to the velocity of the

oscillations. For a vehicle drive-line the main damping effect is achieved from tires. It is very important to find out the resonant frequencies of the drive-line in different operating conditions. A frequency analysis of the drive-line focuses on evaluating the vibrational modes of the system.

The oscillations of the drive-line is evaluated with clutch system engaged, with engine either providing torque to the wheels or motored by the vehicle inertia.

For the aim of this project crankshaft stiffness is not considered, as the main components contributing to drive-line vibrations are the DMF, transmission shafts, axle shafts and tires.

In ?? and ?? vibrational modes of engine and transmission are deployed with disengaged clutch; indeed in this section, the complete powertrain system is analyzed. The case in which the clutch is engaged is the most significant one for the aim of this project, since it highlights the influence of engine and clutch irregularities on the dynamics of the vehicle. This lumped inertia of the system is the total one, in which the engine is added, and of course dependent on the transmission ratio and it becomes higher with high gear ratios. For each gear selected the inertia of the system changes and therefore the vibrational mode. Due to the DMF behavior, the system becomes more complex for frequency analysis. Three operating condition must be considered:

- DMF is not stimulated by enough alternating torque to bring a variation of velocity between the two masses. In this case the DMF acts exactly as a conventional single mass flywheel and it doesnât affect the vibrational behavior of the powertrain. In this condition the free response of the system can be obtained and its main vibrational modes.
- DMF is working in the first stage in which only the springs with low stiffness are operating. Therefore the introduction of this stiffness brings to changes in vibrational modes.
- DMF is working in the second stage since higher torques are exchanged between the two sides of the flywheel and springs with higher stiffness are involved.

Therefore per each gear, these three cases of DMF operation should be considered for a complete frequency analysis. In order to visualize the vibration of the powertrain, a step of torque is applied from the engine. By plotting the output torque on the wheels and the Bode diagram for each gear ratio and DMF condition, the response of the system can be evaluated.

The resonant frequencies result to be higher when the system presents high values of stiffness (DMF in second stage) and low lumped inertia (high gears), and lower with low stiffness (DMF in first stage) and increasing lamped inertia (low gears). As shown in Figura3.42, Figura3.43, Figura3.44, it can be observed that in every working condition, there are two resonant frequencies that are always present. These

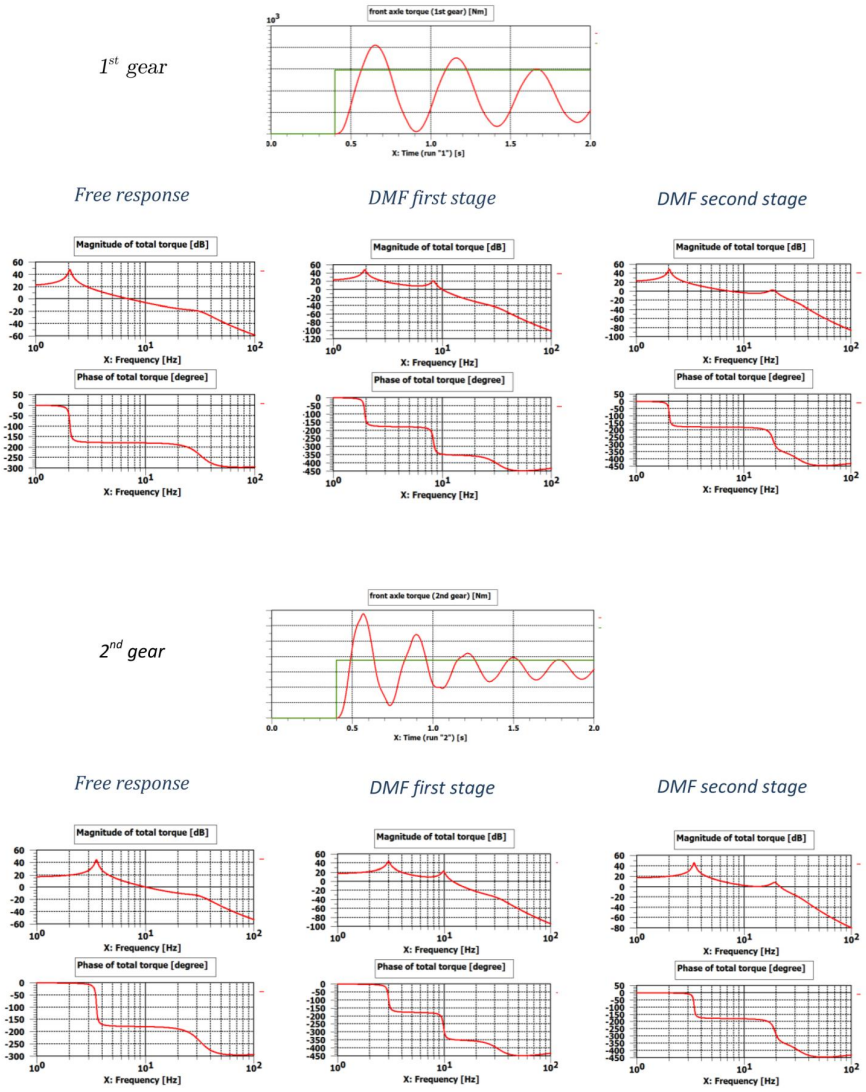

Figura 3.42: Vibrational modes of the vehicle drive-line for gear 1^{st} to 2^{nd}.

frequencies can be found also in the transmission vibrational analysis. Actually their appearance is mainly due to wheels and tire stiffness and can be modified using tires with different properties. It is useful to know when the engine irregularities bring

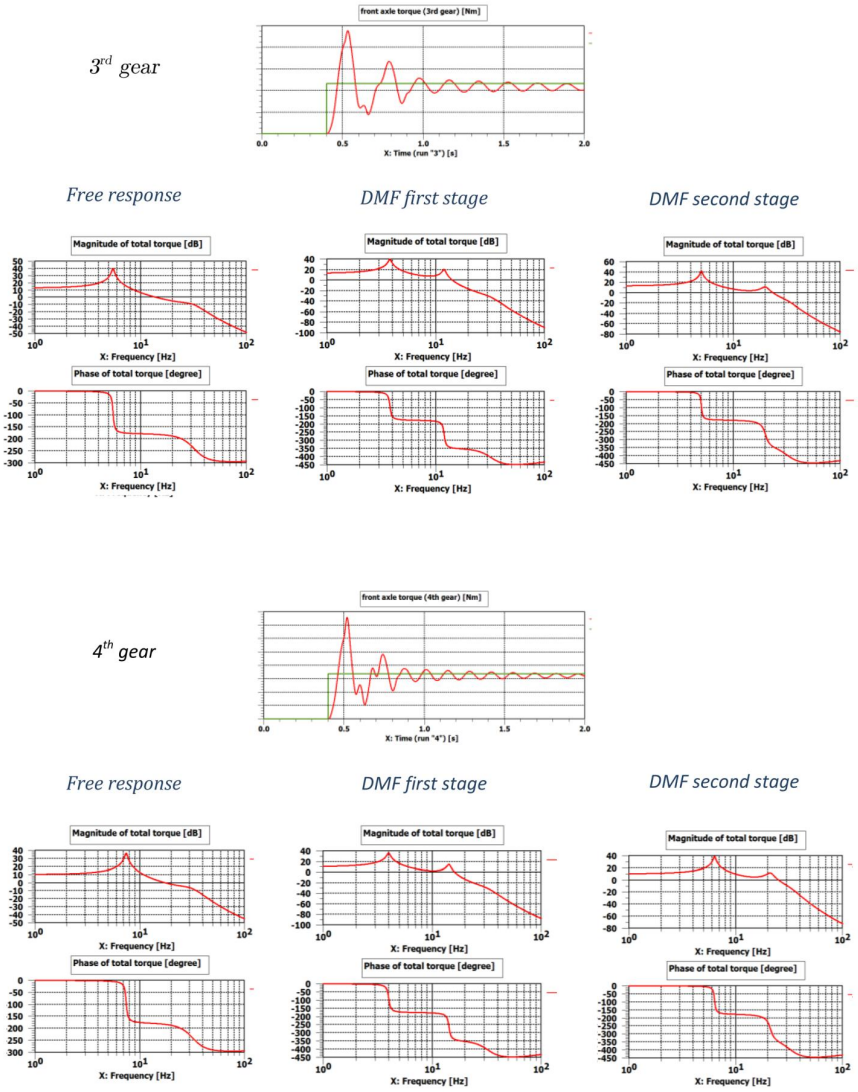

Figura 3.43: Vibrational modes of the vehicle drive-line for gear 3^{rd} to 4^{th}.

the system to work in these resonant modes. As it was already mentioned, if the system undergoes into the resonant fields for a certain amount of time, it can bring to uncontrolled noises and also into failure of some components. When engine speed

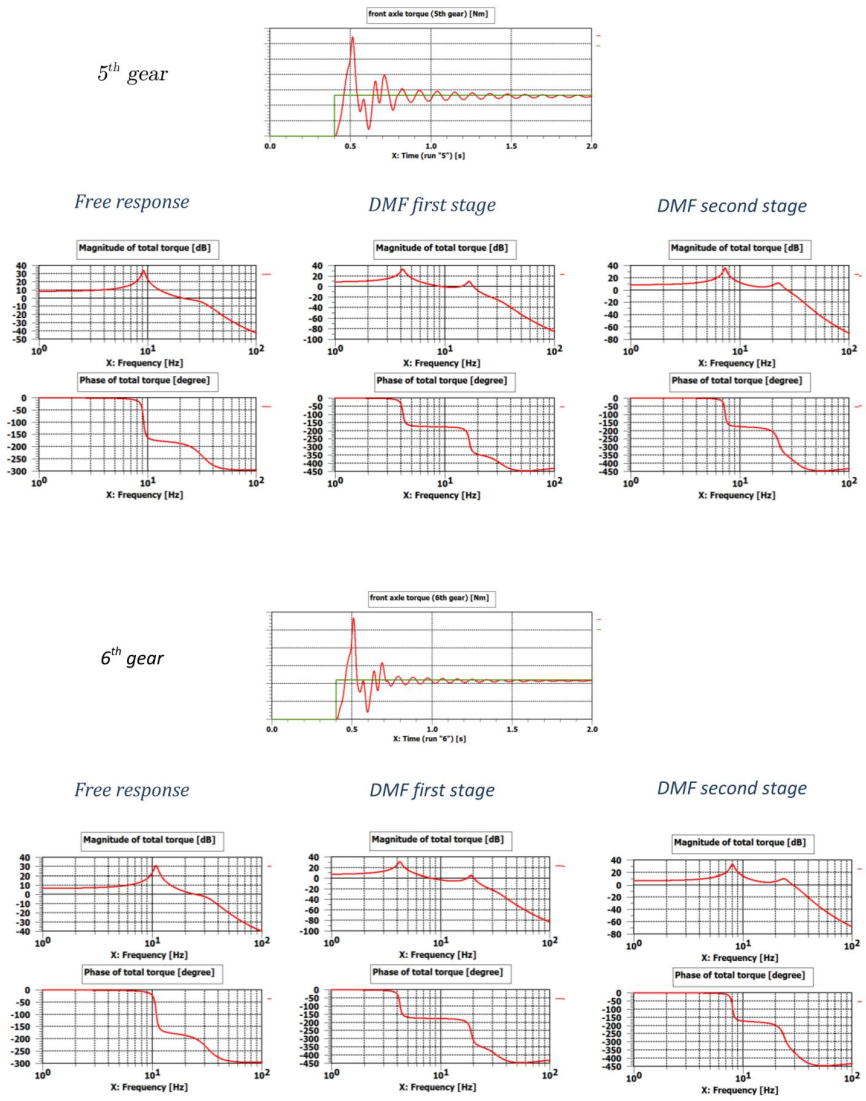

Figura 3.44: Vibrational modes of the vehicle drive-line for gear 5^{th} to 6^{th}.

is close to idle, the power-train is in a critical condition only when high gears (5^{th} and 6^{th}) are engaged and high torque is required (DMF in second stage). Though, this condition happens rarely in real vehicle maneuvers. Actually vibration noises should appear because of tire stiffness. When the engine is running at around 900

rpm the system vibrations tend to be amplified. But this noise is quite well damped by the tire itself. The plot in Figura3.45 shows an example. When the vehicle is travelling at $35km/h$ and the 4^{th} gear is engaged, amplified oscillation can be observed. Instead if travelling at $45km/h$ with the same gear, the oscillations are lower. The resulting vibration on the vehicle acceleration is amplified for a frequency value that matches the tires resonant frequency with respect to other frequencies.

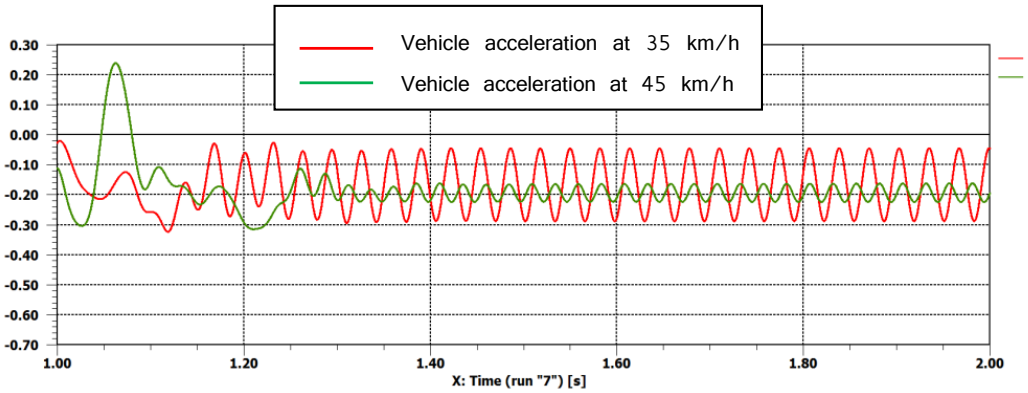

Figura 3.45: Vibration of vehicle acceleration caused by matching tires resonant frequencies.